A Sequential Leaching Protocol for $\delta^{11}B$ and Trace Element Analyses of Multi-Phase Carbonate Rocks

Wei-Li Hong[1,2,3] ⓘ, **Aivo Lepland**[1,2,4,5], **Antoine Crémière**[6,7] ⓘ, **Kalle Kirsimäe**[4], **Eva E. Stüeken**[8] ⓘ, **Matthew Dumont**[8] ⓘ, **Heidi E. Block**[8], and **James W. B. Rae**[8] ⓘ

[1]Geological Survey of Norway (NGU), Trondheim, Norway, [2]Centre for Arctic Gas Hydrate, Environment and Climate, UiT The Arctic University of Norway, Tromsø, Norway, [3]Department of Geological Sciences, Stockholm University, Stockholm, Sweden, [4]Department of Geology, University of Tartu, Tartu, Estonia, [5]Department of Geology, Tallinn University of Technology, Tallinn, Estonia, [6]Division of Geological and Planetary Sciences, California Institute of Technology, Pasadena, CA, USA, [7]Geo-Ocean UMR 6538 CNRS- Ifremer-UBO-UBS, Plouzané, France, [8]School of Earth and Environmental Sciences, University of St. Andrews, St Andrews, UK

Abstract Boron geochemistry from biogenic carbonates offer valuable information about ocean pH and CO_2 chemistry. However, application to geological carbonate deposits suffers from analytical difficulties in obtaining geochemical signals exclusively from the carbonate phase. Sequential leaching with reagents and acids has the potential to overcome such an issue. There is, however, little systematic investigation about the efficiency of sequential leaching in isolating carbonate-associated boron from siliciclastic matrix. Here, we developed a sequential leaching protocol and applied it to methane-derived-authigenic-carbonate samples. Using the leachate $\delta^{11}B$ signatures, elemental composition, and mineral composition of residues, we show that the sequential leaching is able to improve the separation of boron from different phases. Buffered hydrogen peroxide removes organic matter and also some silicate phases resulting low $\delta^{11}B$ values. Leaching with NH_4Ac removes adsorbed boron though may also partially leach some carbonate phases. The first few leaching steps with diluted acetic acid dissolve carbonate phases. Depending on the sample type, these may also capture some remaining adsorbed boron from the preceding NH_4Ac leaching. Once the adsorbed boron is completely removed, as indicated by the progressively higher $\delta^{11}B$ values during the following acid leaching steps, representative carbonate composition can be derived. The accuracy of this protocol is demonstrated with leaching experiments using artificial deep sea coral carbonate and clay mixtures that give the representative carbonate-associated $\delta^{11}B$ within error of the pure coral value. Our results provide insights into characteristic signatures derived from silicates and organic matter that need to be considered in boron isotope analyses of impure marine carbonates.

1. Introduction

Boron geochemistry in biogenic carbonates such as foraminifera and corals, provide a powerful tool to reconstruct carbonate chemistry (Foster & Rae, 2016; Gagnon et al., 2021; Hemming & Hanson, 1992; Hönisch et al., 2019; McCulloch et al., 2018; Shao et al., 2019). However, such an application on other types of carbonate, such as shells, bioclasts or limestones within the rock record, has received comparatively less attention (Jurikova et al., 2019; Kasemann et al., 2010; Stewart et al., 2015). Analyses of bulk rocks, with mixed carbonate and siliciclastic components via bulk digestion is challenging, due to potential contributions of boron from non-carbonate phases, such as finely distributed organic matter and silicate minerals. While in situ methods, such as Secondary Ion Mass Spectrometry (SIMS) and LA-ICP-MS, can analyze a specific spot of the sample, they may simultaneously analyze fine non-carbonate phases, particularly in micritic carbonates, and therefore do not necessarily overcome the problem.

Sequential leaching approaches, that chemically separate different solid phases contained in bulk rocks by using acids and bases of varying strengths and concentrations, provide a promising solution to these issues for a range of isotope systems (Bailey et al., 2000; Bellefroid et al., 2018; Dellinger et al., 2020; Liu et al., 2013; Taylor et al., 2019; Zhang et al., 2017) (Table 1). To date there are only a few studies applying sequential leaching to study boron isotopes and other isotopic systems from carbonates in geological materials (Table 1). For example, Zhang et al. (2017) applied a three-step HNO_3 leaching procedure to study the boron isotopic signatures of shallow marine carbonates composed mainly of calcite and aragonite. Other studies developed sequential leaching protocols for strontium and trace elements in the geological samples. Bailey et al. (2000) developed a

Investigation: Wei-Li Hong, Eva E. Stüeken, Matthew Dumont, Heidi E. Block, James W. B. Rae
Methodology: Wei-Li Hong, Antoine Crémière, Kalle Kirsimäe, Eva E. Stüeken, Matthew Dumont, Heidi E. Block, James W. B. Rae
Project administration: Aivo Lepland
Resources: James W. B. Rae
Supervision: Aivo Lepland, James W. B. Rae
Visualization: Wei-Li Hong
Writing – original draft: Wei-Li Hong, Aivo Lepland, James W. B. Rae
Writing – review & editing: Wei-Li Hong, Aivo Lepland, Antoine Crémière, Kalle Kirsimäe, Eva E. Stüeken, Matthew Dumont, Heidi E. Block, James W. B. Rae

multi-step leaching procedure (acetic acid leaching followed by HCl+HNO$_3$ leaching) to study the $^{87}Sr/^{86}Sr$ ratios in mixed chalk, marl, limestone samples. Extensive acetic acid leaching with 15 different steps was applied on dolostones that include hematite, rutile, clay minerals, quartz, and apatite (Liu et al., 2013) with the emphasis on trace element composition and $^{87}Sr/^{86}Sr$ ratios. A simplified version of this sequential leaching procedure was adopted by Bellefroid et al. (2018) to study $^{87}Sr/^{86}Sr$ ratios in limestone and dolostone. Phillips et al. (2014) applied a two-step leaching with nitric acid of different concentrations to study the pattern of rare earth elements in layers of coal-associated authigenic carbonates. Taylor et al. (2019) recently investigated the effect on dolostone leaching with HCl and acetic acid for Li isotopes and found leaching with weak acids at room temperature has no noticeable contribution from the siliciclastic component.

Here, we examine in detail a previously utilized sequential leaching protocol (Hong et al., 2022), applied to $\delta^{11}B$ in methane-derived authigenic carbonate (MDAC), which provide a useful test material as well as being of geochemical and geobiological interest. MDACs are authigenic carbonates whose precipitation is facilitated by methanotrophic activity in methane-rich sediments (Peckmann et al., 1999; Teichert et al., 2003). The different carbonate minerals, such as aragonite and Mg-calcite, are known to precipitate under distinct fluid conditions as a result of variable seepage strengths and diagenetic influences (Crémière et al., 2016; Himmler et al., 2010; Joseph et al., 2013; Magalhães et al., 2012). MDACs therefore serve as archives of fluid composition changes as recorded in the different carbonates. However, MDAC macrofacies are known to be very heterogeneous due to their intertwined growth with other non-carbonate phases, such as silicates and particulate organic matter (Himmler et al., 2010). Results from bulk geochemical measurements may thus become difficult to interpret as they integrate information from several phases. MDACs are thus an excellent test material for studying how different geochemical signatures may be obtained from mixed-matrix carbonate rocks.

A few studies have investigated $\delta^{11}B$ signatures from MDAC to study the water-rock interaction from an accretionary prism and mud volcanoes (Deyhle & Kopf, 2001, 2004). The same group of authors later identified potential contamination from clay minerals by conducting a series of laboratory experiments (Deyhle & Kopf, 2004), with results highlighting the necessities of a sequential leaching treatment to isolate the B isotope signals from different mineral phases. We show that by applying sequential leaching with oxidants, ion-exchange reagents, and acids of varying concentrations, it is possible to isolate the representative $\delta^{11}B$ and elemental results from carbonate within the mixed matrix composed of silicates and organic matter. While our previous paper (Hong et al., 2022) focused on the interpretation of MDAC $\delta^{11}B$ results as a result of diagenetic modifications from a cold seep setting, this paper focuses on the leaching and calibration of the protocol.

2. Materials and Methods

2.1. Methane-Derived Authigenic Carbonates (MDACs)

We applied a sequential leaching treatment on MDAC samples collected from three cold seep sites along the Norwegian continental shelf, including Vestnesa Ridge (Fram Straight), SW Barents Sea, and the central North Sea (Figure 1a). Aragonite and Mg-calcite are the most common carbonate minerals in the MDAC samples (Crémière et al., 2016). Petrographic characterization of our samples shows that aragonite typically occurs as relatively pure botryoidal cement, filling mm-size cavities (i.e., cavity-filling cement or CFC hereafter) whereas Mg-calcite occurs mostly as microcrystalline cement (i.e., micritic cement or MC hereafter) occupying the pore space of detrital sediments (Figures 1b–1h). MDAC powder was obtained by carefully hand-The drilling into different locations of the MDAC slabs (Figures 1b–1h). The material from different locations on a MDAC slab was mixed and homogenized. Around 35–147 mg of bulk MDAC powder was prepared from both the aragonite and Mg-calcite cemented samples (Table 2). Two sets of experiments with different sediment-to-acid ratios were conducted for the four MDAC samples from the North Sea. For the first set of experiments, ExA, we used 96–137 mg of MDAC with a uniform amount of acid (1.6 ml) and thus higher bulk sediment-to-acid ratios (85–60 mg/ml). Less sediment material, 35–73 mg was used for the second set of experiments, ExB, with lower and variable amounts of acid (0.6–1.2 ml) used among the different acid leaching steps. This results in different sediment-to-acid ratios (42–60 mg/ml for S1 and S2; 56–73 mg/ml for S3 and S4; 114 to 121 for S5 and S6).

2.2. A Leaching Protocol for Geological Carbonate Samples

The leaching protocol consists of three treatments with individual steps within each treatment (Figure 2): (a) an oxidative cleaning with ammonia-buffered peroxide to remove organic material (steps ox1 to ox3); (b) a cleaning

Table 1
Comparison With Previous Sequential Leaching Protocols

	Paris et al. (2010)	Zhang et al. (2017)	Phillips et al. (2018)	Li et al. (2011)	Bailey et al. (2000)	Liu et al. (2013)	Bellefroid et al. (2018)	Hong et al. (2022) and this study-sequential HAc leaching	This study-"one-hit" HNO_3 leaching
Mineral comp./ petrography	Calcite (95%–100%), clay minerals, biosiliceous elements	Aragonite (70%–90%), HMC & LMC (10%–30%)	Siderite (70%–90%), LMC, detrital qz, pla, clay minerals	Limestone, dolostone, phosphorite	Chalk, marl, limestone (74%–98% of $CaCO_3$)	Dolomite, hematite, rutile, clays	LMC, dolomite, limestone,	Aragonite, HMC, with various detrital minerals	
Amount of material used	200 mg	1 mg	100 mg	20–60 mg	100 mg	200 mg	100 mg	ca. 30–150 mg	ca. 8–20 mg
Leaching steps	1	3	2	2 for limestone and dolostone	3	15	7	12	3
Pre-acid leaching steps	No	Buffer: MilliQ, Oxidative: H_2O_2	No	Yes (with HAc or HCl)	Water and 1M of NH_4Ac	5 ml 1N $NH_4Ac+H_2O_2$	7 ml of 1N NH_4Ac	Oxidative: H_2O_2 buffer: NH_4Ac	Oxidative: H_2O_2 buffer: NH_4Ac/5E-4 M HNO_3
Acid used	1.1 ml of 4M HNO_3	<0.5 M HNO_3	5N HAc & 1N HNO_3	ml of 0.2–0.5 M HAc	Tens of ml 20% HAc and 6MHCl + 6M HNO_3	3–5 ml of 0.25%–10% (v/v) HAc	8 ml of 0.04–0.175 M HAc	0.8–1.6 ml of 0.25–10 v% (or 0.0062–1.75 M) HAc	0.1 M HNO_3
Leaching duration	A few hours	NA	A few hours	NA	A few hours to a day		A few hours	A few hours	A few hours
Leaching temperature	Room temp.	NA	100°C	NA	Room temp.	20°C	NA	Room temp.	Room temp.
pH of leachate	NA	NA	NA	NA	NA	2.3–3.1	2.7–3.1	3–6	NA
Target element	B	B	REE/trace elements	Sr	Sr	Sr	Sr	B	B
Range of Al conc. or Al/ Ca ratios	Al: 10^3 ppm	Al/Ca: 31.8–137.4 µmole/mole	Al: 10^3 ppm	NA	NA	NA	Al: 10^1 and 10^3 ppm	Al: 10^1 and 10^3 ppm	Al: 10^1 and 10^3 ppm
Range of Rb conc. or Rb/Sr ratios	NA	NA	NA	NA	NA	Rb/Sr: 10^1–10^2 mmole/mole	Rb: 10^{-1} to 10^{-3} µg	NA	NA
Carb. recovery	NA	NA	NA	~70%	NA	>80%	NA	65.9%–87.9%	4.1%–8.3%

treatment with a buffered solution (1 M NH_4Ac) to remove the adsorbed exchangeable ions from mineral surfaces (steps n1 to n2); and (c) a 10-step acid leaching treatment with 0.25 to 10 vol% acetic acid (HAc, S1 to S10). A fraction of the residue (ca. 5 mg) was sampled between cleaning or leaching treatments and analyzed using X-ray diffraction (XRD) to examine changes in mineral composition after leaching (Figure 2a). All wet chemistry was carried out in a boron-free clean lab at the St Andrews Isotope Geochemistry (STAiG) laboratories at the University of St Andrews.

For the oxidative cleaning, a 3 vol% H_2O_2 solution was prepared by diluting 30 vol% H_2O_2 ten-fold with NH_4OH so that the pH of final reagent is close to 7. Three consecutive oxidative cleaning steps were performed with each step lasting 50–60 min (Figure 2a). Water bath heating (60–70°C) was applied to accelerate the reaction. Bubbling was observed due to oxidation of organic material and care was taken not to make this overly vigorous by avoiding continuous heating instantly after addition of fresh oxidative solution. The leachate was extracted in between the three oxidative cleaning steps after centrifuging the solid and fluid mixture at 12,000 rpm (rotations per minute) for 10 min. These extracts were transferred into acid-cleaned micro-centrifuge tubes and kept for
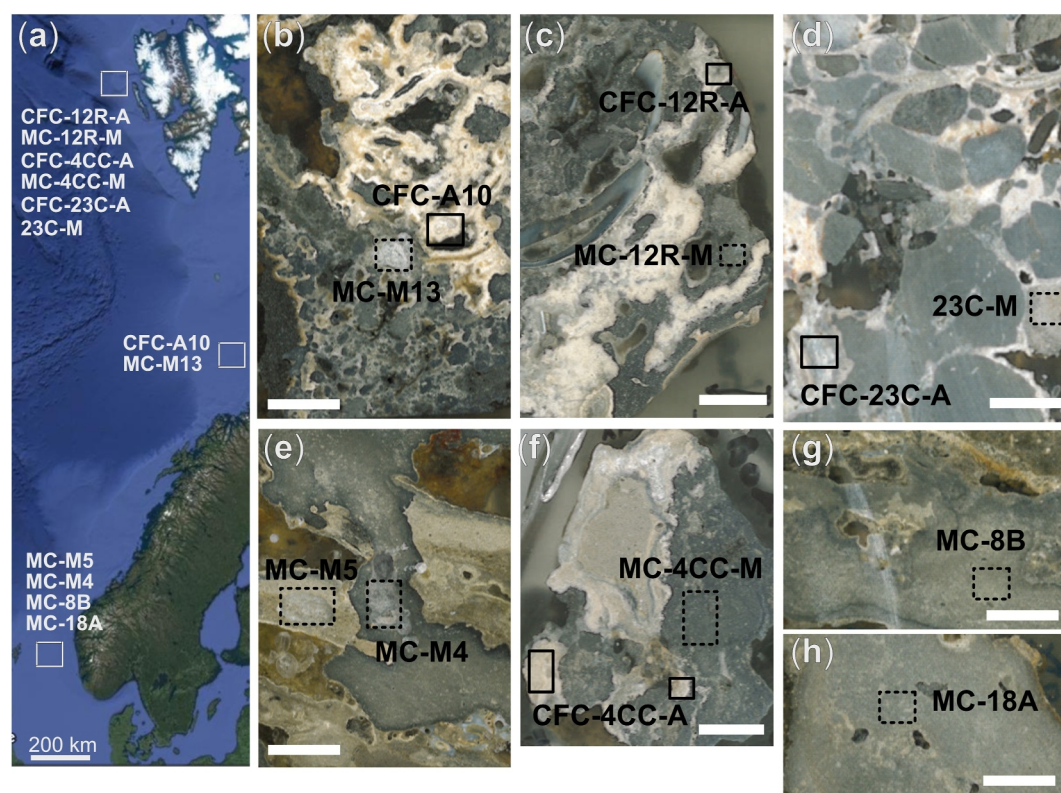
Figure 1. Locations and photos of samples for leaching from methane-derived authigenic carbonate slabs modified from Hong et al. (2022). (a) The 12 samples were collected from Vestnesa Ridge (Fram straight), North Sea, and Barents Sea. (b–h) The Samples of cavity-filling cement (CFC) and micritic cement (MC) carbonates were taken from squares with solid and dashed boarders, respectively. Sample 23C-M in (d) was collected from the siliceous matrix and contains essentially no carbonate.

subsequent analyses. Fresh 3 vol% H_2O_2 solution was added to the samples after the removal of leachate. At the end of the oxidative cleaning treatment, bubbling ceased and the residual solid was washed three times by first mixing the residual solids with Milli-Q deionized water (18.2 MΩ cm) and then separating the solution from the solids by centrifuging.

The oxidative cleaning was followed by two consecutive buffer cleaning steps (n1 and n2; 0.5 M NH_4CH_3COO or NH_4Ac; pH ~ 7; Figure 2a). The purpose of such cleaning is to remove any adsorbed materials from the mineral surfaces. The buffer cleaning was performed at room temperature for ca. 30 min per step. Similar to the oxidative cleaning treatment, the leachate was extracted in between each buffer cleaning step by centrifuging twice. Three washes with Milli-Q deionized water were performed after the buffer cleaning. A fraction of the solid was removed for XRD investigation after the Milli-Q water wash. This solid fraction was dried in clean laminar flow hood overnight to remove excess moisture.

The 10-step CH_3COOH (HAc) leaching treatment included five different concentrations: 0.25 vol% (S1–S4), 0.5 vol% (S5–S6), 1 vol% (S7–S8), 5 vol% (S9), and 10 vol% (S10) (Figure 2a). No Milli-Q wash was performed in between the steps. The leachate from each step was extracted from the vial by centrifuging twice as described in the oxidative and buffer solution cleaning steps. A fraction of the wet powder was removed for XRD between steps in the same fashion as described earlier.

A deep sea coral (Lophelia pertusa S09397, or LPC hereafter, collected live from 626 m water depths on Rosemary Bank) was drilled and homogenized. This was mixed with a carbonate-free deep sea clay, taken from the base section of a multicore from CDISK4 Station 1: 22N, 158W, 4,725 m water depths, <0.04% PIC, Steiner et al., 2022), to make artificial mixtures containing 25%, 50%, and 75% carbonate (25%, 50%, and 75%-carb hereafter). Due to the small quantity of artificial mixtures (ca. 16–41.6 mg, Table 3), as compared with the

Table 2
List of Samples and Their Mineral Composition

Carb piece sample #	Lab ID	Area	Material used (mg)	Recovery[a]	XRD-carbonate (%)				XRD-detrital (%)			
					Arg	Cal	Dol	Qz	K-Fsp	Pl	Mca	Chl
P1210007-C	A10	Barents Sea	63.6	**40.3 mg**/NA/NA	NA	NA	NA	NA	NA	NA	NA	NA
P1210007-C	M13	Barents Sea	62.0	**15.1 mg**/NA/NA	NA	NA	NA	NA	NA	NA	NA	NA
13C-1F	M4	North Sea	136.6(ExA) 35.4(ExB)	**48.8 mg**/63.2 mg/77.2%	43.1	3.2	4.9	38.4	4.2	4.3	1.9	BD
13C-1F	M5	North Sea	127.1(ExA) 33.4(ExB)	**51.9 mg**/64.4 mg/80.1%	42.8	7.9	BD	38.5	7.1	2.2	1.4	BD
13C-CARB-8-B	8B	North Sea	118.4(ExA) 68.5(ExB)	**44.5 mg**/50.6 mg/87.9%	25.0	17.7	tr.	46.0	6.5	3.4	1.4	BD
13C-CARB-18-A	18A	North Sea	96.2(ExA) 72.5(ExB)	**28.4 mg**/41.8 mg/67.9%	BD	43.5	BD	46.9	3.7	3.7	2.2	BD
P1606-23C	23C-A	Vestnesa Ridge	47.7	NA	74.0	22.1	BD	2.5	0.7	BD	0.5	BD
P1606-23C	23C-M	Vestnesa Ridge	52.9	NA	BD	BD	BD	93.7	1.6	BD	0.8	3.7
21616-1-4CC	4CC-A	Vestnesa Ridge	37.6	NA	78.3	14.0	BD	3.5	1.2	BD	2.9	BD
21616-1-4CC	4CC-M	Vestnesa Ridge	145.2	**75.8 mg**/115.0 mg/65.9%	73.1	6.1	BD	12.4	1.2	1.2	5.9	tr.
21637-1-12R	12R-A	Vestnesa Ridge	39.7	NA	86.7	7.2	BD	3.0	1.6	BD	1.1	BD
21637-1-12R	12R-M	Vestnesa Ridge	146.5	NA	75.1	5.7	BD	9.2	2.2	1.2	6.7	BD

Note. Arg: aragonite; Cal: calcite; Dol: dolomite; Qz: quartz; K-Fsp: K-feldspar; Pl: Plagioclase; Mca: Mica; Chl: chlorite; BD: below detection; tr.: non-quantifiable trace amount; NA: not available. [a]Recovery was calculated based on the amounts of calcium carbonate leached (bold numbers), the weight of raw material used, and the percentage of Arg+Cal determined by XRD (underlined numbers). Recoveries for most of the Vestnesa Ridge samples are not available as only part of the HAc leaching was applied to these samples.
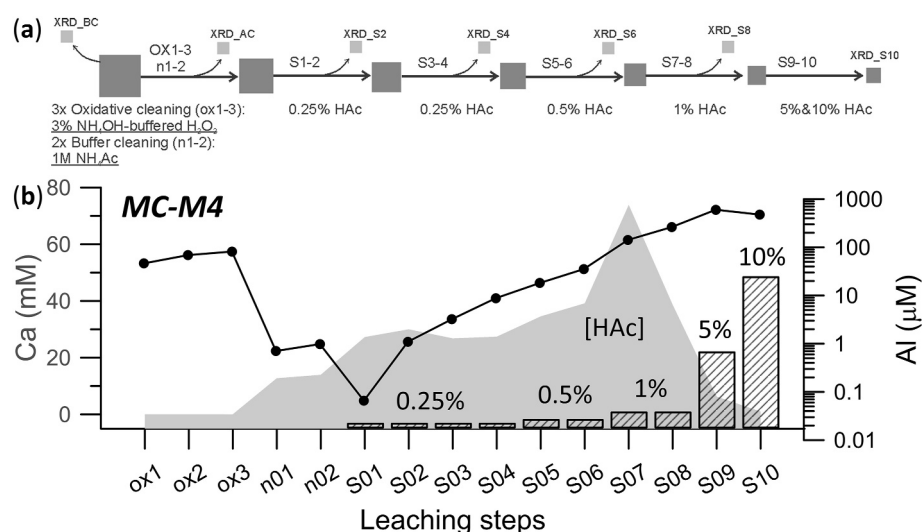
Figure 2. A schematic diagram showing our sequential leaching protocol. (a) The different steps of leaching and timing when sample materials were collected for XRD inspection. XRD_BC: XRD sample taken before cleaning (i.e., without any treatment). XRD_AC: XRD sample taken after oxidative and buffer cleaning. (b) The concentrations of Ca (light gray polygons) and Al (black line with dots) in leachate from MC-M4 were shown alongside to demonstrate the progressive dissolution of carbonates. Shaded bars indicate concentrations of HAc used in different leaching steps.

Table 3
Leaching Experiment of Clay-Carbonate Mixtures With Known Composition

	Reagent vol. (ml)	Clay (mg)	$CaCO_3$ (mg)	Expected boron[a] (nmole)	Boron recovery[b]	$CaCO_3$ recovery[c]	B/Ca[d] (μmol/mol)
25%-carb	0.375	15.9	5.3	35.0	87%	69%	833
50%-carb-1	1.5	8.0	8.0	53.3	115%[e]	101%	
50%-carb-2	0.75	10.9	10.9	72.4	84%	74%	754
50%-carb-3	1.5	20.8	20.8	138.4	88%	76%	770
75%-carb	1.5	5.0	15.0	99.9	97%	89%	726
100%-carb	1.5	0	20.0	133.2	92%	84%	729
LPC-1	NA	0	3.52	23.0	NA	NA	654
L-2	NA	0	2.73	18.5	NA	NA	679

Note. NA: not applicable. [a]Calculated from the average boron content of L and adjusted to the amounts of $CaCO_3$ used for each of the mixtures (see Data Set S2, https://doi.org/10.60520/IEDA/113483 for values). [b]Calculated from the expected boron and the summation boron in the leachates from buffer cleaning to S7. [c]Calculated from the amounts of $CaCO_3$ mixed and the summation calcium in the leachates from buffer cleaning to S7. [d]B/Ca ratios were calculated considering the variable boron and carbonate recovery of the different samples, where the ratios for LPC-1, LPC-2, and JCp-1 were determined analytically and reported in Data Set S2, https://doi.org/10.60520/IEDA/113483. [e]The over recovery may be due to addition of boron from silicate phases as the reagent-to-carbonate ratio is not optimal for this experiment. No B/Ca ratio was thus calculated for this sample.

amounts used for the MDAC samples (35.4–136.6 mg, Table 2), we adjusted reagent volumes according to the clay-to-carbonate ratios to weaken leaching power when less carbonate is in the sediment mixture (see Table 3 for the reagent volumes). Pure coral carbonate samples (100%-carb hereafter) were also treated following the same leaching protocol. In addition, we applied an established cleaning procedure (Rae et al., 2011) on LPC (in duplicate) and a widely used coral reference material (JCp-1, Gutjahr et al., 2021) whose $\delta^{11}B$ values were then compared with the values obtained from 25%, 50%, 75%, and 100%-carb samples.

The entire leaching was also applied to four samples from the North Sea (MC-M4, MC-M5, MC-8B, MC-18A) and two samples from Barents Sea (CFC-A10 and MC-M13). For the remaining six samples from Vestnesa Ridge, the only up to acetic acid leaching steps S6 were applied (i.e., excluding steps S7–S10). Though the Vestnesa Ridge samples were cleaned with buffered and oxidative reagents, not all the leachate composition from these cleaning steps are available. As a comparison, we also performed bulk HNO_3 leaching from four of the samples (MC-M4, MC-M5, MC-8B, and MC-18A).

2.3. Major/Trace Element and $\delta^{11}B$ Analyses

An aliquot of leachate was analyzed for major and trace elements either on an Agilent 7500 ICP-MS (for MDAC samples) and an Agilent 8900 ICP-MS (for the artificial samples) in the STAiG laboratory. Analytical methods followed previously published protocols (Ni et al., 2007; Rae et al., 2011), though avoided use of NH_3 in the spray chamber. Instead, a wash solution of 0.5 M HNO_3 + 0.3 M HF was used to improve washout of boron (Misra et al., 2014; Zeebe & Rae, 2020), which required the use of an "inert" sample introduction system, including a self-aspirating PFA (perfluoroalkoxy alkane) nebulizer, a PFA spray chamber, and a sapphire injector.

TCa concentration in the solution was measured to determine the dilution factor for boron isotope analyses. Samples were diluted to matrix-match samples and standards at 1 mM Ca concentration. Blanks and standards were measured every three samples. Background correction was carried out by on-peak zeroing, using the average of the bracketing blanks. Blank-corrected values were converted to absolute concentrations by sample-standard bracketing against a trace element solution standard, which has a composition that mimics marine $CaCO_3$. Consistency standards were interspersed throughout the run to check for accuracy and precision. Long-term reproducibility was ~2% (2RSD) on element/calcium ratios in the mmol/mol range, and ~5% in the μmol/mol range. Rb concentrations were determined separately on an Agilent 8900 ICP-QQQ-MS with the same protocol as the other elements. Absolute concentrations were determined by correcting against a matrix-matched in-house standard produced by adding Rb single-element solution to a pre-existing standard. Average reproducibility of two further in-house standards measured across two separate runs was 2.5% (2RSD).

Depending on the concentration of B in each sample, 500–1,000 μl of the leachate was passed through gravity columns of boron-specific anionic exchange resin Amberlite IRA 743 (Kiss, 1988; Yoshimura et al., 1998) to

isolate 2–10 ng of B following the procedure detailed in Foster (2008) and Xu et al. (2024). Samples from the mixed coral carbonate-silicate tests were purified following an updated batch purification protocol (Trudgill et al., 2024). The pH in leachates S1–S6 was between five and six; these samples therefore required no additional pH adjustment before loading onto the resin. For leachate S7–S10, samples were mixed with equal volumes of NH_4Ac buffer to adjust the pH to values higher than five before the separation. A few wash solutions from the oxidative and buffer cleaning steps were also purified without additional pH buffering, as these have pH greater than five. There were high concentrations of boron in the solutions from the oxidative cleaning; therefore 30–100 µl of the solutions was sufficient to isolate sufficient boron for isotopic analyses. A procedural blank solution (100 µl 5% HAc + 400 µl Milli-Q water + 500 µl 0.5 M NH_4Ac) and a NIST (National Institute of Standard and Technology) carbonate standard solution (25 µl 0.5 M RM8301c + 58 µl Milli-Q water + 50 µl 0.5 M NH_4Ac; Stewart et al., 2021) were processed with every set of 8–10 samples to monitor contamination and reproducibility during chemical purification. The elution tail of each column-purified sample was checked with an additional column rinse with 0.5 M nitric acid to ensure complete elution of boron in the sample. Boron isotopic signatures were analyzed with a Thermo Finnigan Neptune MC-ICP-MS, following Foster (2008) and Rae et al. (2011), but with the use of 0.3 M HF to improve boron washout from the spray chamber, as described in Rae (2018), Shao et al. (2019), and Trudgill et al. (2024). Purified samples were scanned for Na, Mg, and Ca to check for efficient removal of sample matrix and buffer prior to B isotope analysis. Blank correction was performed by on-peak zeroing, and mass bias correction by sample-standard bracketing with NIST 951. Boric acid consistency standards, AE121 and BIGD (Foster et al., 2013; Stewart et al., 2021; Vogl & Rosner, 2012), were run with every batch as a check on accuracy and instrument precision. Long-term reproducibility during the analytical campaigns was 0.13‰ for AE121 (2SD with an average of 19.63‰, $n = 33$), 0.19‰ for BIGD (2SD with an average of 14.81‰, $n = 10$), and 0.36‰ for 8301C (2SD with an average of 24.19‰, $n = 33$).

2.4. XRD Analyses

The mineral composition of MDAC samples was studied by XRD in the laboratory of Department of Geology, University of Tartu. Minute samples were pulverized by hand with an agate pestle and mortar under ethanol and preparations were made by dropping the sample suspension on low-background Si wafers. Dried preparations were scanned on a Bruker D8 Advance using CuKα radiation and LynxEye position sensitive detector in 2–70° 2Θ range with step size 0.012° and counting time 1 s per step. The semi-quantitative mineralogical composition of the samples was interpreted and modeled using the Rietveld algorithm-based code Topaz by Bruker. Due to small sample size (5–7 mg) the relative error of quantification is ca. 20%.

3. Results

Information about the MDAC samples used and their mineral composition are listed in Table 2. The XRD results for the residual powder sub-sampled between leaching steps are listed in Data Set S1 (Hong et al., 2024). Elemental composition and $\delta^{11}B$ values of the different cleaning and acid leaching steps are reported in Data Set S2 (Hong et al., 2024). Cross plots of elements released during the different steps were presented in Figures S1–S3 of the Supporting Information S1.

3.1. XRD Results

Based on the mineral composition of the 12 investigated samples, the samples fall into three groups (Figure 3):

– Group 1: more than 50% detrital minerals with variable fractions of aragonite and Mg-calcite
– Group 2: predominately aragonite (>75%) with a small fraction of Mg-calcite (6%–22%) and siliciclastic minerals (4%–19%)
– Group 3: one sample consists of entirely detrital minerals (23C-M).

Samples MC-A10 and MC-M13 have not been analyzed by XRD. However, based on the elemental ratios from the leachate (see Section 3.3), the results from Crémière et al. (2016) as well as visual inspection on where the samples were drilled, those two MDAC samples likely belong to Group 1.

The residual solids after the different leaching steps were also examined with XRD to investigate the mineral composition changes (Figure 4 and Data Set S1, https://doi.org/10.60520/IEDA/113483). Due to the large uncertainty in the mineral abundance determined by XRD, we can only make qualitative assessment of the changes
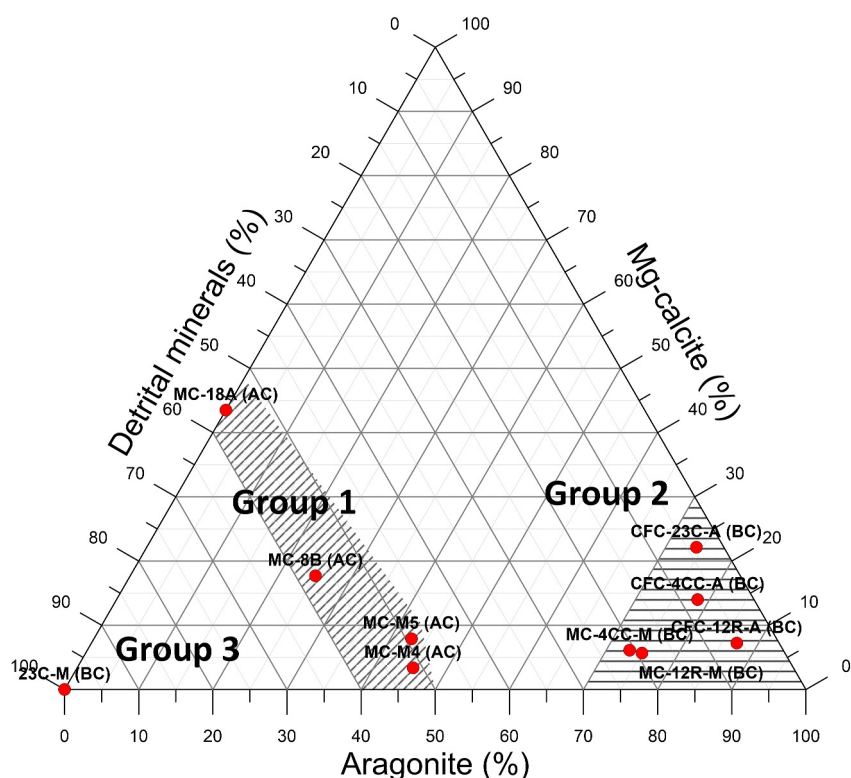
Figure 3. Mineral composition of the samples investigated. Three groups were defined based on the mineral assemblage. *BC*: sample material without any treatment. *AC*: sample material gone through oxidative and buffer cleaning (see Figure 2 for the protocol).

in mineral abundance. Nonetheless, our XRD results are still useful in determining the presence of minerals. We normalized the abundance of aragonite, calcite, and bulk non-carbonate fraction to quartz, which is assumed to be unaffected by our diluted HAc leaching. It is apparent that both calcite/quartz and aragonite/quartz ratios decrease as the leaching progresses, while the quartz-normalized bulk silicate mineral abundances are unchanged within analytical error during sequential leaching.

3.2. Validation of the Leaching Protocol With Artificial Mixtures of Carbonate and Clay of Known Boron Geochemistry

For all samples, high recoveries of carbonate (86%–109%) were calculated from the Ca concentrations in buffer cleaning and HAc leachates (S1–S9). Recoveries of 84%–101% of carbonate-bound boron were also calculated by comparing with the boron content from the LPC samples. The $\delta^{11}B$ values obtained from the first seven HAc leaching steps of the 100%-carb sample are in a good agreement with the values obtained from LPC (Figure 5a) that serve as a procedure blank for our wet chemistry treatments. For the different mixed samples (i.e., 25%, 50%, and 75%-carb), $\delta^{11}B$ values agree with the LPC values from the buffer cleaning steps (n1 and n2) and the first two diluted HAc leaching steps (S1 and S2, Figures 5b–5e). These results suggest no detectable fractionation of boron during the proposed leaching treatment. Dissolution of silicate phases (higher Al/Ca ratios and lower $\delta^{11}B$ values as compared to those from LPC) can be observed when leaching with more concentrated HAc at the later stages (Figure 6a). Leachates from oxidative cleaning contains much higher B/Ca ratios compared to the HAc leaching steps (Figure 6b), a result of boron release from organics and/or silicates (Al/Ca ratio $\sim 10^4$–10^5 µmol/mol, Data Set S2, https://doi.org/10.60520/IEDA/113483) with minimal leaching of carbonate.

To explore the influence of variations in reagent and sample quantities, three different volumes of reagent versus carbonate mass were tested for the 50%-carb sample (Table 3). In the test with the highest reagent-to-carbonate ratio (0.185 ml/mg, 50%-carb-1 in Figure 5d), the buffer cleaning steps yield $\delta^{11}B$ values characteristic of the pure carbonate sample, whereas the HAc steps are offset to lighter values with lower Ca and elevated Al concentrations
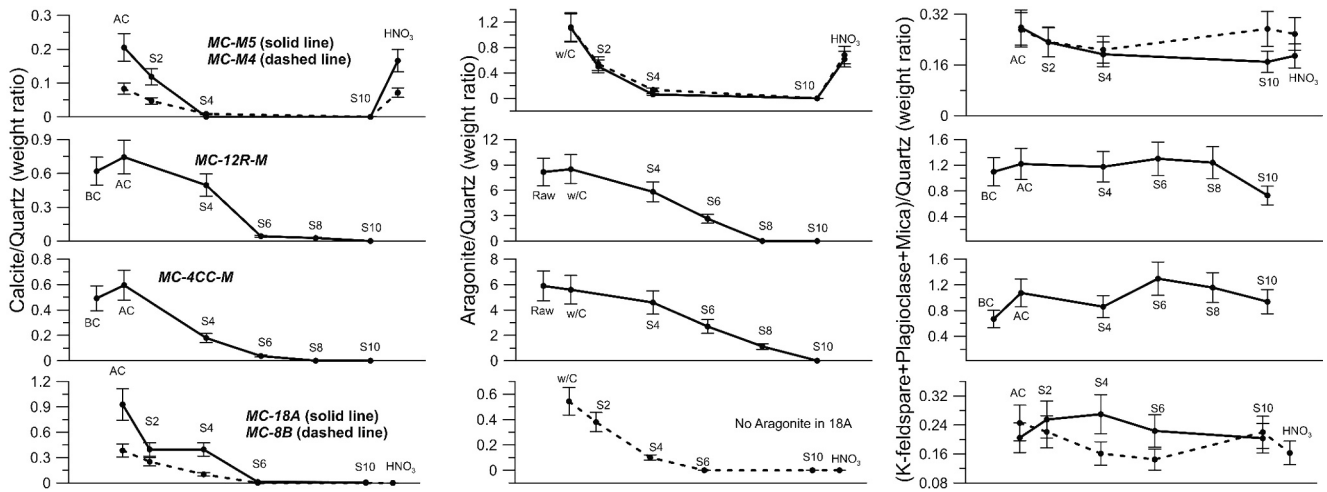
Figure 4. Mineral composition of the residual sediments from the different leaching steps. Only selected micritic cement samples were inspected with XRD (see Data Set S1, https://doi.org/10.60520/IEDA/113483 for detail). For the three cavity-filling cement samples (CFC-23C-A, CFC-4CC-A, and CFC-12R-A), quartz-normalized ratios were not presented due to the highly variable values as a result of only trace amounts of quartz in these samples. The abundance of different mineral phases was normalized to quartz whose abundance is assumed to be unaffected by the leaching. In general, the abundance of calcite and aragonite of the matrix samples decreases throughout leaching with relatively unaltered silicate phases.

(Figure 6a), suggesting exhaustion of the carbonate and increasing influence from silicate leaching. When reagent-to-carbonate ratios of 0.069–0.100 ml/mg $CaCO_3$ was adopted, the first two HAc leaching steps were able to extract representative carbonate $\delta^{11}B$ values (50%-carb-2 and 50%-carb-3 in Figures 5e, 5f, and 6a), regardless of the absolute amounts of clay and carbonate in the sediment mixtures used (Table 3). The slightly elevated Al content and lower $\delta^{11}B$ values of 50%-carb-3 may suggests some minor contamination from silicate phases, but this is substantially less than in the case of non-optimized reagent-to-carbonate ratio. The B/Ca ratios calculated for these clay-carbonate mixtures are higher than the two LPCs (Table 3), which is likely due to the different
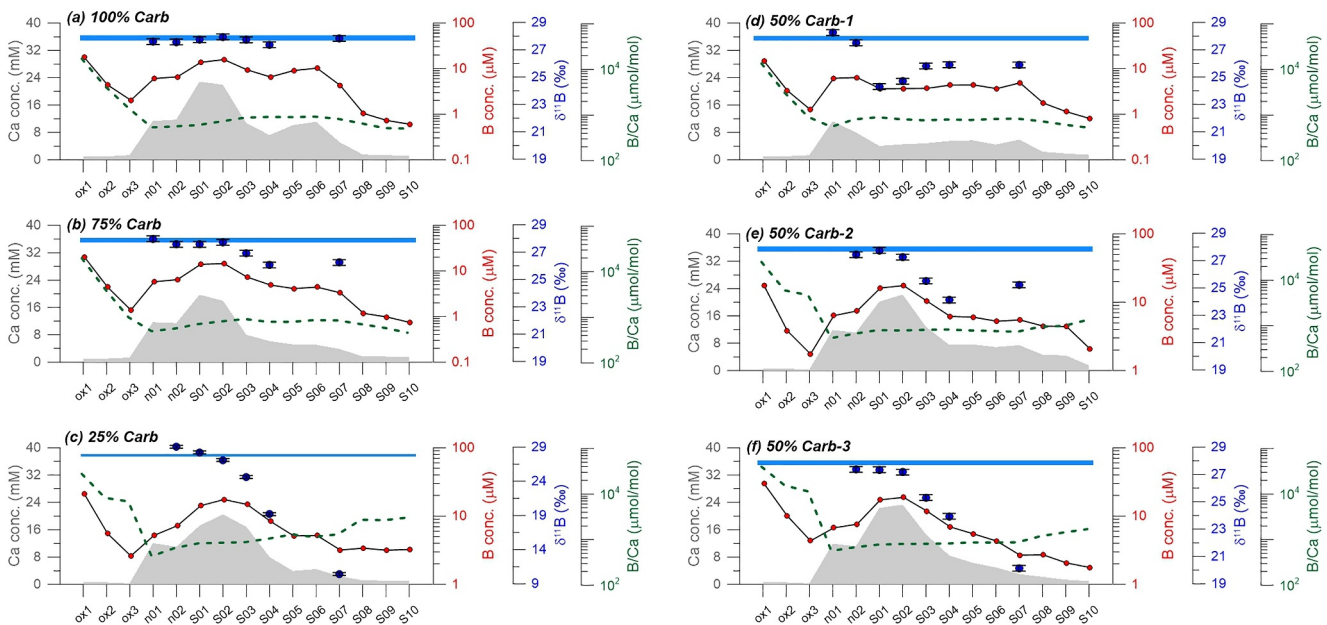
Figure 5. Ca concentrations (gray polygons), B concentrations (red dots), and B/Ca ratios (green dashed lines) of the different leaching steps for the mixed carbonate samples with known $\delta^{11}B$ values as marked by blue lines (+27.8 to +27.9‰). X-axes mark the different cleaning/leaching steps. Notice the different scale for $\delta^{11}B$ from (c).
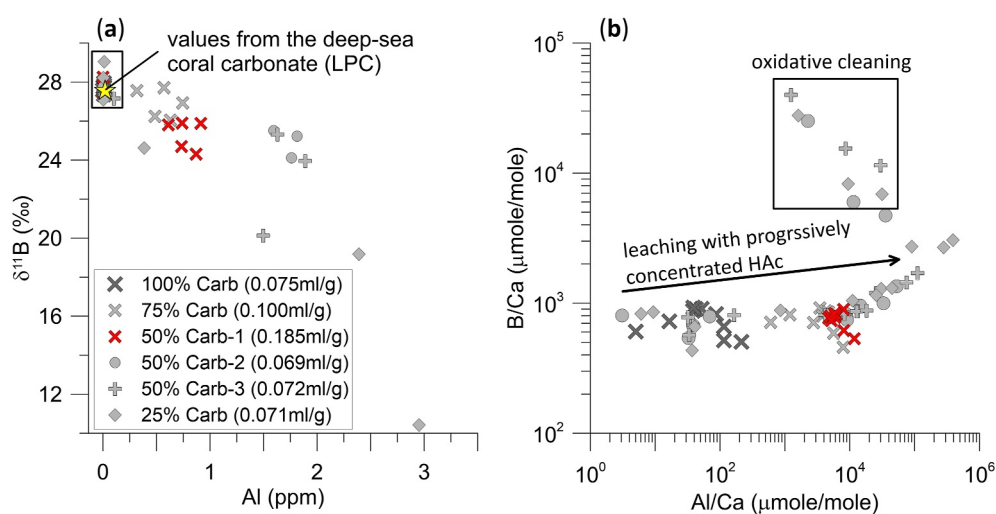
Figure 6. Leachate $\delta^{11}B$ and composition from the artificial experiments. (a) $\delta^{11}B$ versus Al content for the different sets of experiment. The similar $\delta^{11}B$ values derived from the different experiments, as compared to the values from LPC, validate our leaching protocol. (b) Higher Al/Ca ratios in leachates indicate higher contributions of silicate phases at leaching steps with more concentrated HAc. The high B/Ca and Al/Ca ratios from oxidative cleaning indicates these elements from organic matter and/or potential silicate phases.

recovery of boron and carbonate. Through these collective results, we conclude that our proposed sequential leaching protocol is able to extract representative $\delta^{11}B$ of carbonate from clay-carbonate mixtures.

3.3. Leachate Composition From Oxidative Cleaning, Buffer Cleaning, and HAc Leaching of the MDAC Samples

Less than 0.1 mM of Ca is detected in the oxidative cleaning solutions (steps ox1 to ox3 in Figure 7), while the Ca concentrations are three orders of magnitude higher in the buffer cleaning (n1–n2) and HAc leaching steps (S1–S8). Regardless of the variable carbonate content in the MDAC samples, fairly constant Ca concentrations (12–14 mM) are observed in the buffer cleaning solution from the six samples with available data (MC-M5, MC-M4, CFC-A10, MC-M13, MC-8B, and MC-18A in Figures 7–9). For the HAc leaching steps, the Ca concentration systematically increases as more concentrated HAc leaching was applied until the available carbonates in samples were fully dissolved. The Ca concentrations are usually highest at S7 or S8 and rapidly decrease in the last two steps. The recovery of carbonate through the sequential HAc leaching (i.e., S1–S10) from MDAC samples can be calculated by comparing the amounts of Ca in the leachate and the XRD results and assuming that the Ca is mainly carried by carbonates (Table 2). Leaching was able to dissolve 28.4–75.8 mg of carbonates, equivalent to recoveries of 65.9%–87.9% (n = 5) (Table 2). About 6%–10% of carbonate was dissolved during the buffer cleaning.

The concentration of Al in the leachate, a tracer for aluminosilicate minerals, varies by two to three orders of magnitude throughout the entire leaching process, with the highest concentrations observed either from the oxidative cleaning or from the last two acid leaching steps (Figure 7). Al concentrations also vary widely between different samples, with the highest concentration observed from MC-4CC-M and the lowest concentrations from CFC-4CC-A, CFC-12R-A, and CFC-23C-A, the three samples that contain the least detrital material based on our XRD inspection (Figure 3). Rb concentrations, which trace clay influence (Bellefroid et al., 2018; Liu et al., 2013; Table 1), were analyzed for six of the samples (Figure 7). Rb concentrations are mostly lower than 0.3 μM with occasional higher concentrations from buffer cleaning steps in samples MC-8B and MC-18A. From the HAc leaching steps, higher Rb concentrations are observed in the steps with strong acid. The variation in Rb concentrations is much lower as compared to that for Al.

The concentrations of B vary by two to three orders of magnitude between the different treatments (Figure 8). Highest B concentrations (11.7–50.1 μM) are observed from the first oxidative cleaning step and gradually decrease in steps ox2 and ox3 (Figure 8). Lower B concentrations are generally observed from the buffer cleaning
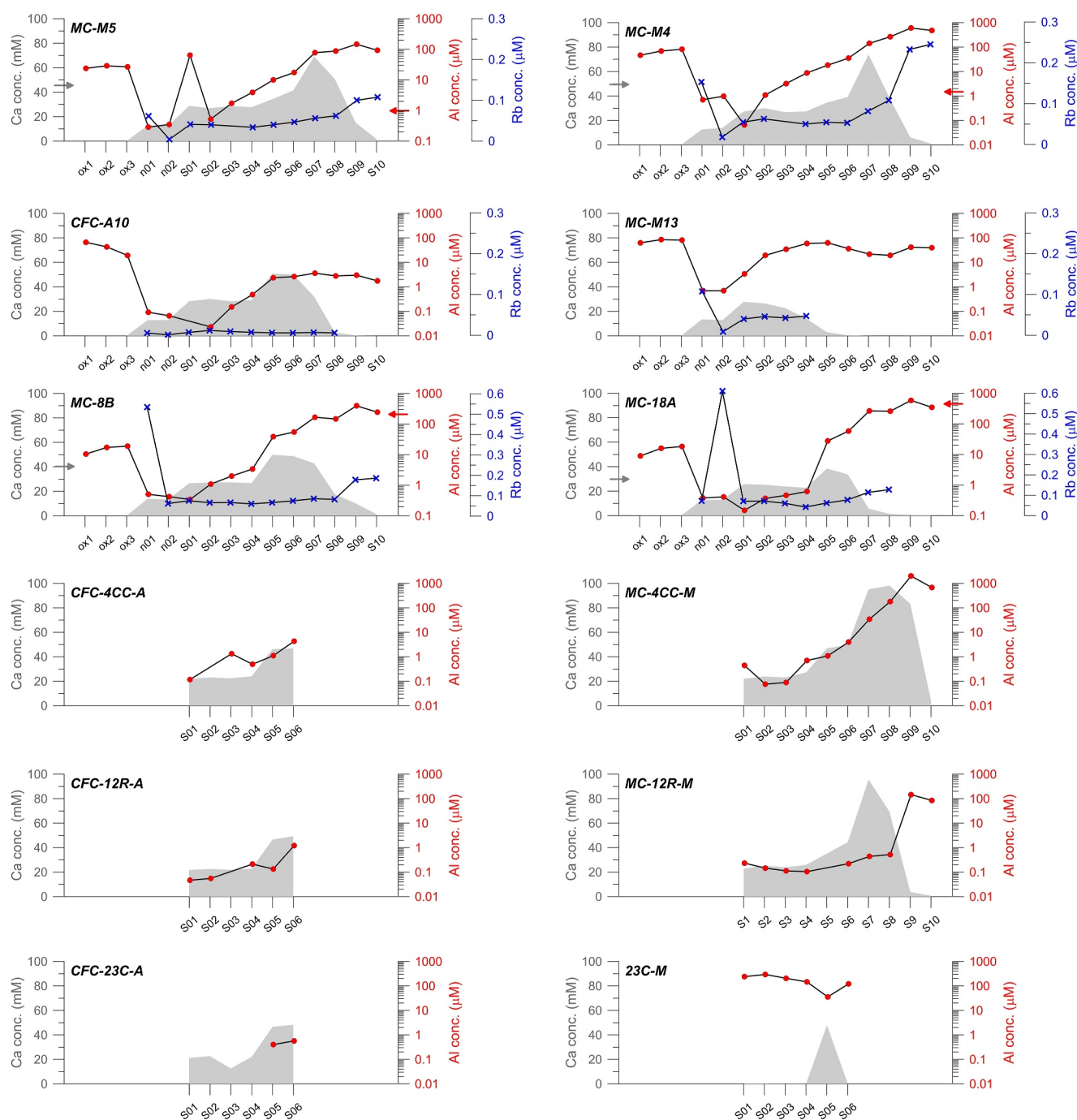
Figure 7. Ca concentrations (gray polygons), Al concentrations (red dots) and Rb concentrations (blue crosses) of the different leaching steps for the 11 MDAC samples and one background sediment sample (23C-M). The red and gray arrows next to the Al and Ca axes, respectively, indicate the concentrations from a single-step HNO_3 leaching for MDAC samples MC-M4, MC-M5, MC-8B, and MC-18A.

and first acid leaching steps. In general, the concentration of B is proportional to the concentration of Ca in the leachate between S1 and S7 or S8; that is, relatively constant B/Ca ratios are observed among these steps (green dash lines in Figure 8). Despite the rapid decreases in Ca concentrations for S9 and S10, considerable amounts of boron are still detected in some MDAC samples during leaching with concentrated acids. Boron isotopic compositions vary in some samples by almost 10‰ across the entire leaching treatment (such as from CFC-A10, MC-M13, and MC-18A), though often with relatively coherent values in the HAc leaching steps. $\delta^{11}B$ values from the
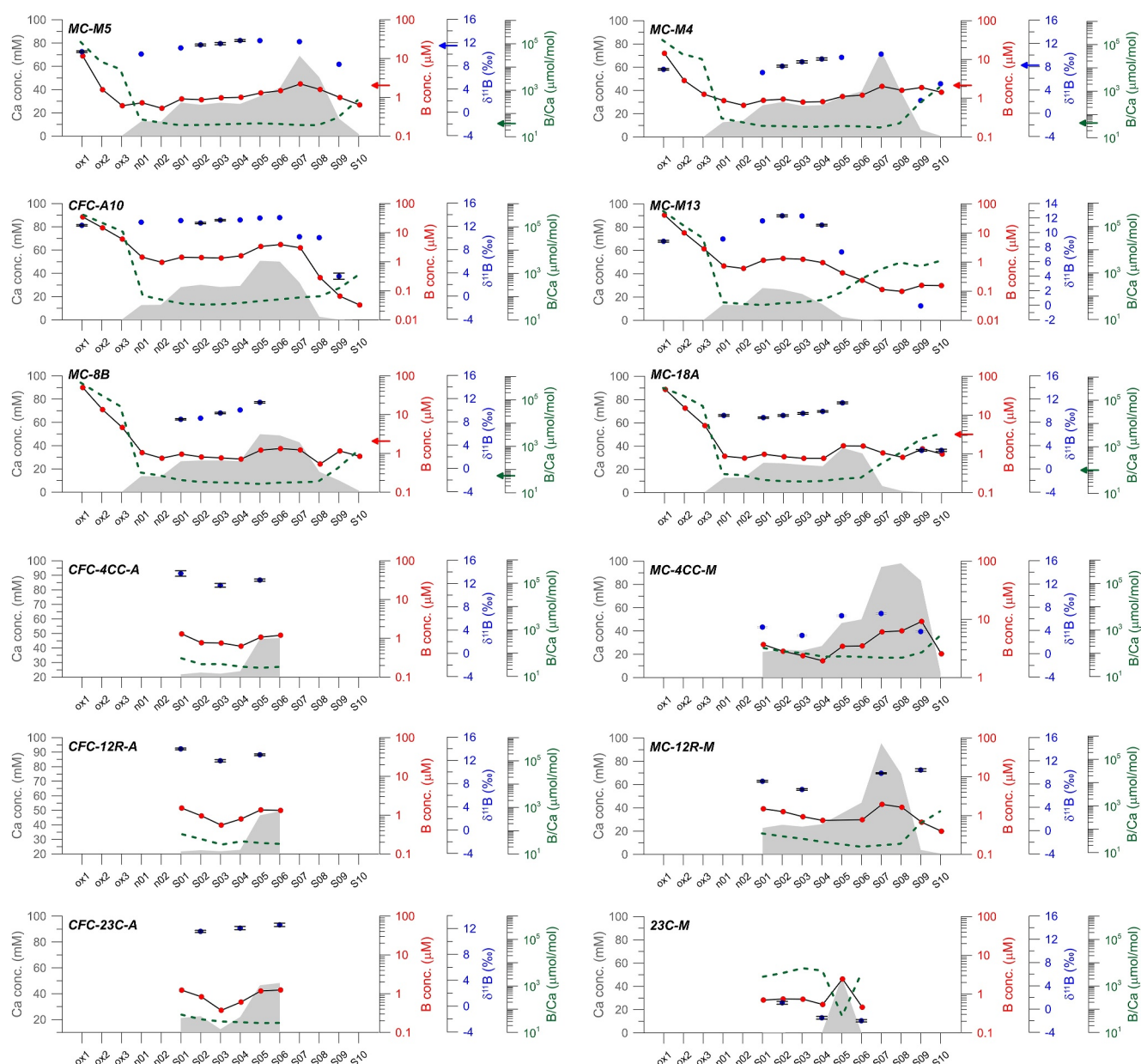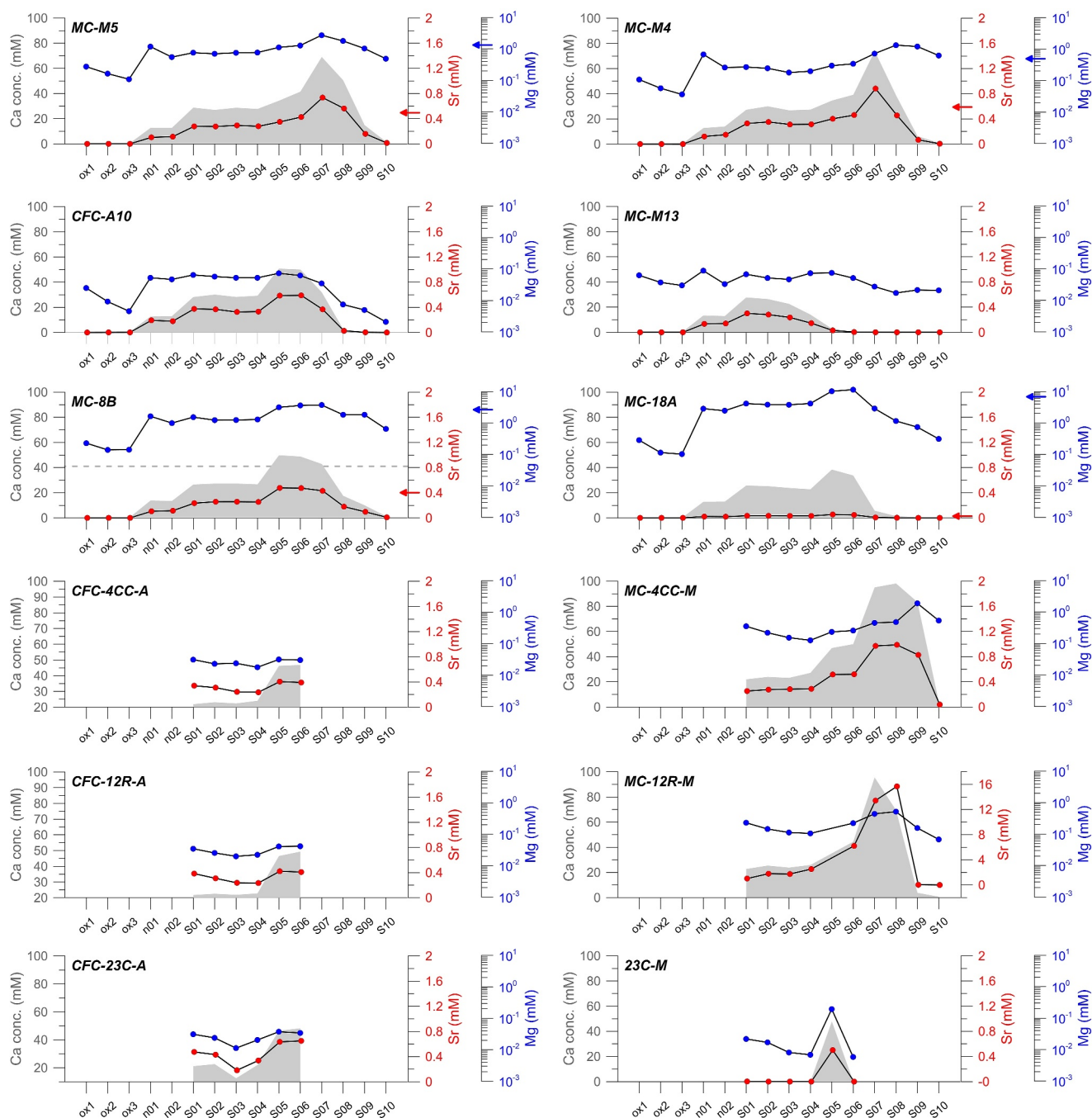
Figure 8. Ca concentrations (gray polygons), B concentrations (red dots), B/Ca ratios (green dashed lines) and $\delta^{11}B$ (blue dots) of the different leaching steps for the 11 MDAC samples and one background sediment sample (23C-M). The red, blue, and green arrows next to the B, $\delta^{11}B$, and B/Ca axes, respectively, indicate the concentrations and ratios from a single-step HNO_3 leaching for MDAC samples MC-M4, MC-M5, MC-8B, and MC-18A. No $\delta^{11}B$ values are available for the HNO_3 leaching from MC-8B, and MC-18A.

oxidative and buffer cleaning steps are usually slightly lower than the values from HAc leaching. Gradual increases in $\delta^{11}B$ values from S1 to S7 or S8 are usually observed, followed by a large decrease in $\delta^{11}B$ values from S9 and S10. The lowest $\delta^{11}B$ value is observed from sample 23C-M, the sample mostly composed of silicate minerals with very little carbonate (Figure 8).

Sr and Mg concentrations in leachate are plotted along with Ca concentrations in Figure 9. Low concentrations of Sr were detected from the oxidative cleaning, while, in buffer cleaning and acid leaching steps, Sr concentrations track Ca concentrations in leachate, resulting in similar Sr/Ca ratios across these steps (Data Set S2, https://doi.org/10.60520/IEDA/113483). High concentrations of Mg were already detected in the oxidative cleaning steps, even though the values are still lower than those from buffer cleaning and acid leaching. From the last few steps of

Figure 9. Ca concentrations (gray polygons), Sr concentrations (red dots), and Mg concentrations (blue dots) of the different leaching steps for the 11 MDAC samples and one background sediment sample (23C-M). The red and blue arrows next to the Sr and Mg axes, respectively, indicate the concentrations from a single-step HNO_3 leaching for MDAC samples MC-M4, MC-M5, MC-8B, and MC-18A.

acid leaching, despite the rapid decrease in Ca concentrations, Mg concentrations remain relatively high, indicating a non-carbonate phase was being dissolved (Figure 9).

To investigate how the variable sediment-to-acid ratios may affect the leaching efficiency, four samples were tested (Figure 10). We observe fairly similar $\delta^{11}B$ values between the ExA and ExB, the experiments with different sediment-to-acid ratios, for samples MC-8B and MC-18A (Figure 10). For samples MC-M4 and MC-M5, the $\delta^{11}B$ values are substantially higher for the ExB as compared to that for ExA. Taking sample MC-M4 as an example, $\delta^{11}B$ values from S1 to S4 in ExB are consistently around +10‰ while the $\delta^{11}B$ values for ExA
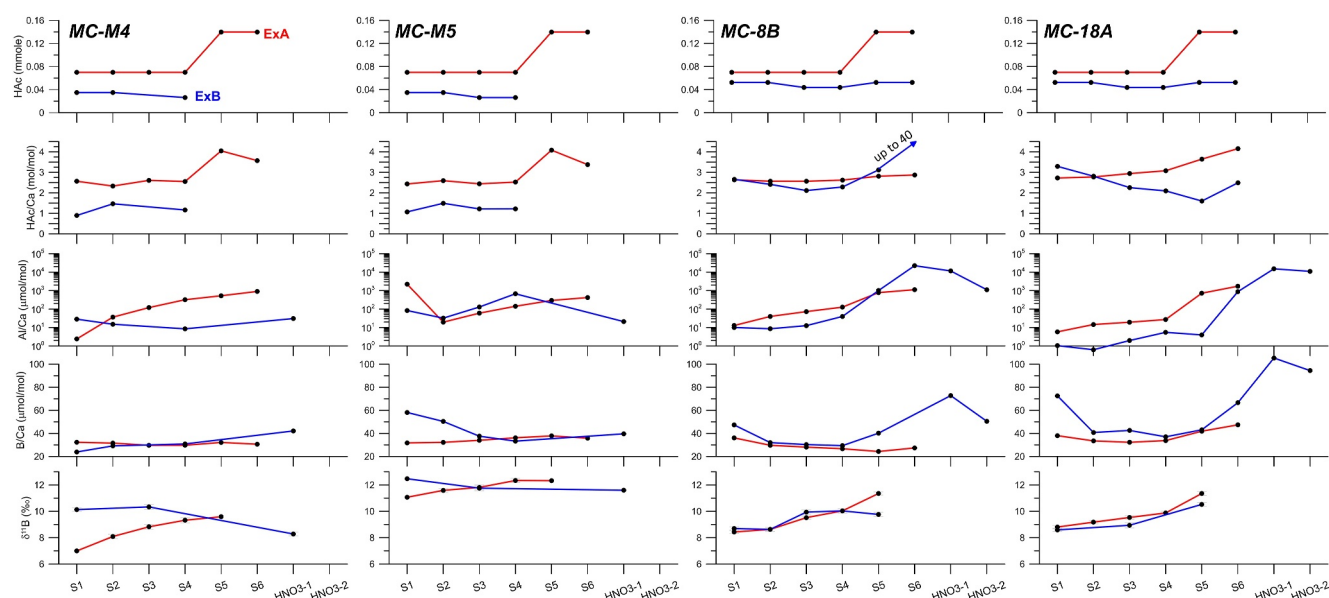
Figure 10. The effect of sample amount and acid volume on leaching results. The four columns show the different MDAC samples leached during steps S1–S6 by different amounts of acid used during ExA (red) and ExB (blue) sessions. The moles of HAc in the first row were calculated from the concentration of HAc, the volume of HAc used in each step, the density of HAc (1.05 g/ml), and the molecular weight of HAc (60.05 g/mol). Based on the ratios of Sr/Ca and Mg/Ca, identical carbonate phases where leached for the four MDAC samples during the two sessions. $\delta^{11}B$ signatures are lower for samples M4 and M5 analyzed during ExA which may be due to the higher excess HAc. All $\delta^{11}B$ signatures, however, approach a common value when leaching progresses.

increase from +7‰ (S1) to +10.2‰ (S7), which is attributed to the greater release of adsorbed B from clay when more sample material was used in ExA (see Section 4.1 for more discussion). The B/Ca ratios are also different between ExA and ExB, particularly in the early leaching steps, with higher ratios in S1 for samples M5, 8B, and 18A from ExB (Figure 10). Such a difference cannot be correlated to the amounts of excess HAc used, the Al/Ca ratios derived, and their $\delta^{11}B$ values. For sample M4, the B/Ca ratios are very similar between the ExA and ExB despite the high excess acid in the former experiment. Despite these variations, B/Ca ratios approach a common value between ExA and ExB when more acid leaching steps were applied. Collectively, the comparison of ExA and ExB, along with the 50%-carb experiments described in Section 3.2, suggest that careful design of leaching approach is important to obtain reliable element ratios and $\delta^{11}B$ values.

4. Discussion

4.1. Sources of Boron From the Oxidative and Buffer Cleaning Steps

The solid phases that were leached during the different steps are examined through the elemental composition as well as the $\delta^{11}B$ of the leachate. Hydrogen peroxide (H_2O_2) is commonly used to oxidize organic matter in soil and sediments (Mikutta, Kleber, Kaiser, & Jahn, 2005). The efficiency of organic matter removal has been shown to depend on solution pH with less than 20% removal in alkaline (pH 9–10) solutions (Hosking, 1932). During oxidative cleaning, our solution pH was near neutral, a condition that should allow 50%–90% of organic matter to be removed (Mikutta, Kleber, & Jahn, 2005) while also preventing substantial dissolution of calcium carbonates, consistent with the very low concentration of calcium in these solutions (Figures 5 and 7).

Boron concentrations are the highest in the oxidative cleaning steps (compared to other treatments) while $\delta^{11}B$ values (+7.6 to +12.2‰) are slightly lower compared to HAc-leaching steps (Figure 8). Similar observations can be made from the leaching of deep sea clay and coral carbonate mixtures. Boron concentrations are consistently high in the leachate of the first oxidative cleaning step with very high B/Ca ratios (Figure 6b). The boron adsorbed onto organic matter at pH 5–9 has been shown to be isotopically light (Lemarchand et al., 2005), around 25‰ lower compared to the values in the solution (which is seawater or porewater in our case), likely in part due to preferential interaction with the isotopically light borate ion. The boron desorbed from organic matter during oxidative cleaning is therefore expected to carry $\delta^{11}B$ values of ca. +15‰; however, this notably higher than what was measured from our oxidative cleaning leachate (+7.5 to +12.2‰; $n = 4$). Boron from organic matter

alone may not explain the observed isotopic signatures from the oxidative cleaning steps. A boron source with lower $\delta^{11}B$ signature is required, such as from the decomposition of silicate minerals, consistent with the high concentrations of Al detected when leaching our MDAC samples (Figure 7) and artificial samples (Figure 6a). It is therefore likely that partial silicate mineral dissolution may be, to some degree, responsible for the high B concentration and low $\delta^{11}B$ signatures in the oxidative cleaning. While we cannot pinpoint the exact silicate phase responsible, we note that isotopically light B has been observed in—and may be relatively easily leached from—phyllosilicates (for instance biotite with $-42.4 \pm 1.6‰$ (Voinot et al., 2013)) and could therefore explain this observation.

The buffer cleaning with NH_4Ac is expected to remove elements from exchangeable sites on the mineral surfaces. Bailey et al. (2000) showed that such treatment may also partially dissolve calcite and remove weakly complexed Ca. This conclusion is consistent with the appreciable Ca and Sr concentrations measured from these steps, which are about half of what were measured from the acid-leaching steps (Figure 9). Concentrations of Al, Li, and Na are much lower compared to the oxidative cleaning steps, which suggests no significant dissolution of silicate minerals (Figure 7 and Figure S2 in Supporting Information S1). The $\delta^{11}B$ values from the buffer cleaning leachate are within the range of $+9.2$ to $+12.7‰$ for the MDAC samples ($n = 5$). Desorbed B from clay minerals is known to have $\delta^{11}B$ values 20–30‰ lower than the solution (Palmer et al., 1987), or ca. $+10$ to $+20‰$ with seawater/porewater as the co-existing solution. Such a range in $\delta^{11}B$ agrees with what we measured and suggests a primary contribution from clay desorption during the buffer cleaning as expected.

Partial dissolution of carbonate is also observed in the buffer cleaning steps of the artificial clay-carbonate mixtures, as indicated by the indistinguishable $\delta^{11}B$ values from the values of LPC (Figure 5). In the case with a high reagent-to-carbonate ratio (e.g., 50%-carb-1), these steps exhaust much of the available carbonate, leading to substantial contamination from other non-carbonate phase(s) during HAc leaching. For example, nearly half of the carbonate was dissolved during the two buffer cleaning steps (n1 and n2, Figure 5d) for the 50%-carb-1 sample. With the low remaining quantity of carbonate, the boron associated with other non-carbonate phases contribute substantially to the HAc leachate and results in $\delta^{11}B$ values lower than the expected values from LPC (Figure 5d).

4.2. Deriving Representative Boron Signatures From Carbonates With Sequential HAc Leaching

During HAc leaching steps S1–S6, carbonate was dissolved with an increasing yet minor contribution from silicate mineral dissolution, as indicated by the low concentrations of Al and Rb (Figure 7). The highest $\delta^{11}B$ values are generally seen in the samples with the highest calcium content; these are found in the initial S1–S2 steps in the artificial clay-carbonate mixtures, while in the MDAC samples, the $\delta^{11}B$ gradually increases from the values observed in the buffer cleaning steps toward the highest values when $\sim40\%$–60% of the carbonate was dissolved (e.g., between S3 and S6; Figure 8). We attribute this increasing $\delta^{11}B$ trend to a decreasing contribution of adsorbed boron from non-carbonate phases that was not removed during the buffer cleaning. When progressively more concentrated acid is applied during mid-stages of leaching, the boron released from carbonate dissolution gradually dominates the signal and results in the highest $\delta^{11}B$ signature between steps S3 and S6 in the various samples. A similar observation has been made by Bailey et al. (2000) when investigating Sr systematics in carbonates (Table 1). They showed that a significant amount of Sr associated with non-carbonate phases was liberated during leaching with less-concentrated acids. In their study, complete removal of such an unwanted Sr signal was achieved when $\sim40\%$ dissolution of carbonate was reached (Bailey et al., 2000). Assuming analogous B behavior, we would expect complete removal of such contaminant boron during minor acid leaching, for example, before steps S3 and S6.

The exact acid leaching step in which the highest $\delta^{11}B$ value appears depends on both the carbonate content as well as the sediment-to-acid ratios in each sample (Figure 10), as also demonstrated in our leaching of artificial samples (Figures 5d–5f). A large quantity of sample material means that there are more exchangeable sites from clay surfaces for B, which is extracted in the early stage of the acid leaching and thus lowers the $\delta^{11}B$ signatures. The lower $\delta^{11}B$ values derived from steps S1 to S4 during ExA session for MC-M4 and MC-M5 likely reflect a significant input of this clay-derived boron. Only at step S5 was all the adsorbed B removed unmasking the carbonate signal. When a smaller quantity of sample material is used for leaching, such as in ExB, most of the clay-adsorbed boron was removed early in the leaching treatment and thus the boron from carbonate dissolution becomes the dominated component already in S2 or S3.

It is important to note that the volume and/or the concentrations of acid needed should be adjusted according to the sample quantity, so that not all carbonate is dissolved in the first few steps of acid leaching. Otherwise, the leachate from acid treatment in the later steps may contain increasing amounts of boron from the co-occurring silicates (see below for further discussion). Despite the effect of sample material quantity, the $\delta^{11}B$ values derived from the two sessions converge (e.g., S4 and S5 for samples MC-M4 and MC-M5; Figure 10). This is in accordance with our conclusion that the highest $\delta^{11}B$ values derived from the sequential leaching likely approach the primary carbonate signal.

The lower $\delta^{11}B$ values observed from S1–S4 as compared to S5 and S6 support our inference that a significant fraction of exchangeable B can still be present and released in the acid leaching steps with less-concentrated acids. Nonetheless, another potential explanation may be the release of boron that re-adsorbed to clay surface during HAc leaching steps, as there are still substantial amounts of dispersed clay minerals that could serve as exchangeable sites for B. In other words, it is possible that some of the carbonate-bound boron released during the earlier acid treatment steps is immediately re-adsorbed to clay surfaces and is released during the following steps at higher acid strength. Consequently, the measured $\delta^{11}B$ value of a given leachate may be lower than the genuine carbonate value due to the adsorbed B. However, we anticipate very little re-adsorption onto clays due to the low pH of the leachate, even for the 0.25% HAc (pH between five and six). No adsorption is expected for pH lower than 5.40 as the adsorption coefficient K_D ($=\frac{[B]_{sed}}{[B]_{solu}}$) is essentially zero when considering the linear correlation between pH and K_D reported by Palmer et al. (1987). A calculation to quantify such an effect on adsorption during acid leaching is given in Supporting Information S1. The result of this calculation supports our conclusion, as does the lack of such a trend in the artificial clay-carbonate mixtures.

In acid leaching steps with concentrated HAc (i.e., S7–S10), relatively little carbonate is left, as indicated by the low Ca concentrations from these steps (Figure 8). Boron concentrations either maintain similar levels as in the preceding leaching steps or drop to lower values (Figure 8). The $\delta^{11}B$ values gradually decrease toward the values derived from 23C-M, the sample entirely composed of non-carbonate phases (−2 to +1‰, Figure 3 and Table 4). Such a trend in B suggests a shift in sources from dissolution of carbonate to silicate materials, such as pelagic clay whose $\delta^{11}B$ can be as low as −6.6‰ (Ishikawa & Nakamura, 1993). Such a conclusion is also supported by the high Al and Rb concentrations detected in these steps (Figure 7).

Based on the HAc leaching results, we conclude that the steps with the highest $\delta^{11}B$ values during sequential leaching provide the most representative values for carbonates. Depending on the abundance of carbonate and the applied sediment-to-acid ratios, the highest $\delta^{11}B$ values may occur at acid leaching steps S3–S6 (Table 4), or earlier for our leaching of artificial samples (Figure 5). Occasionally, the highest $\delta^{11}B$ values were observed from steps S2 (MC-M13) and S7 (MC-4CC-M and MC-12R-M), which can be explained by either the low carbonate content in a small quantity of sample used for MC-M13 or the high carbonate content in a large quantity of sample used for MC-4CC-M and MC-12R-M. For example, a single step of acid leaching (i.e., S1) is sufficient to remove most adsorbed B from MC-M13 as a result of the low carbonate content (as estimated from Ca concentration in leachate; Figure 8) and a small quantity of sample material used (62 mg; Table 2). In contrast, samples MC-4CC-M and MC-12R-M contain the most carbonate of all the MDAC samples (92.3% and 95.9% of bulk material, respectively; Table 2) and also have larger quantities of material (145.2 and 146.5 mg, respectively; Table 2). As a result, additional acid leaching (i.e., up to S6) is required to completely remove the adsorbed B and obtain an end member carbonate signal. Such a conclusion can be strengthened by comparing the trends of $\delta^{11}B$ and Ca concentrations: leachates with the highest $\delta^{11}B$ usually corresponding to the steps with the highest Ca concentrations (Figure 8).

From the leaching of artificial clay-carbonate mixtures, we are able to provide a practical suggestion for the quantity of reagent required to optimally leach a given amount of carbonate in the sediment. Representative $\delta^{11}B$ of carbonate are obtained from the first two 1.5 ml volume HAc leaching steps in the 75%-carb sample (Figure 5b) that contains ca. 15 mg of pure coral carbonate (Table 3). However for the 50%-carb-1 sample, which has only 8 mg carbonate, $\delta^{11}B$ from the 1.5 ml volume HAc leaching steps are substantially lower than that from LPC, indicating the amount of carbonate is too low to survive buffer cleaning steps of this volume and concentration. A minimum of 15 mg pure carbonate in the samples can therefore be suggested as the lowest quantity needed for the volume/concentration of regent used following the proposed leaching procedure (i.e., 1.5 ml of reagent per step, with concentrations as in Figure 2). If samples with lower carbonate content are used, then the reagent volume should be scaled appropriately. For example, we are able to obtain representative carbonate $\delta^{11}B$ values from the

Table 4
Representative Elemental Ratios and $\delta^{11}B$ Values for the Samples Investigated

MDAC spl	Ca (mM)	Al (µg)	Li/Ca (µmole/mole)	B/Ca (µmole/mole)	Na/Ca (mmole/mole)	Mg/Ca (mmole/mole)	Al/Ca (µmole/mole)	Mn/Ca (µmole/mole)	Sr/Ca (mmole/mole)	Cd/Ca (µmole/mole)	Ba/Ca (µmole/mole)	Nd/Ca (µmole/mole)	U/Ca (nmole/mole)	$\delta^{11}B$ (‰)	f_{Si}[a] (%)	Corr-$\delta^{11}B$ (‰)	Corr-B/Ca (µmole/mole)	Corr-Mg/Ca (mmole/mole)	Sequential leaching steps considered[b]
CFC-A10	50.4	0.1	6.5	72.0	9.8	1.3	49.4	15.9	11.7	BD	26.8	0.3	3,769.3	13.5	0.3	13.5	71.8	1.3	S5–S6
MC-M13	26.4	0.8	9.4	50.6	9.2	1.9	731.6	31.4	10.7	BD	14.8	0.1	2,806.6	12.3	5.5	13.1	47.9	1.9	S2
MC-M5	30.2	0.1	9.5	47.2	5.2	32.6	112.6	44.6	9.9	BD	39.8	BD	1,617.2	12.4	1.0	12.6	46.8	32.6	S1[c]&S4
MC-M4	22.5	>0.1	8.8	30.9	4.3	9.5	8.5	43.7	12.1	BD	25.0	0.1	282.5	10.3	0.1	10.3	30.8	9.5	S3–S4[c]
MC-8B	49.8	1.7	13.1	24.3	4.4	63.3	779.3	80.3	9.6	0.1	39.9	0.3	430.6	11.4	12.1	13.2	21.4	63.6	S5
MC-18A	38.4	1.2	29.2	41.9	2.5	266.8	722.4	185.5	1.4	0.1	39.5	1.3	485.9	11.4	6.5	12.3	39.2	266.7	S5
CFC-23C-A	48.2	>0.1	5.1	25.8	4.4	0.7	11.8	99.6	13.5	BD	115.2	BD	303.9	12.6	0.2	12.6	25.8	0.7	S6
CFC-4CC-A	46.2	>0.1	3.9	23.1	5.0	0.7	24.0	6.2	8.8	BD	28.0	BD	784.9	12.6	0.4	12.6	23.0	0.7	S5
MC-4CC-M	95.0	1.5	25.2	64.2	7.9	4.8	361.8	81.7	10.2	0.1	28.8	0.3	2,520.8	6.9	2.1	7.1	62.8	4.8	S7
CFC-12R-A	46.5	>0.1	3.8	29.4	4.8	0.9	2.9	3.4	9.1	BD	23.9	BD	1,257.0	13.0	<0.01	13.0	29.4	4.8	S5
MC-12R-M	95.4	>0.1	1.0	20.4	54.7	4.6	4.6	2,076.7	140.8	10.5	0.1	30.3	0.9	9.9	0.1	9.9	22.0	6.0	S7–S8
23C-M	0.1	5.3	1,847.6	3,951.2	16.7	50.1	1.04E6	3,916	1.3	2.6	384.7	57.4	1,876	−2.0					S6

Note. BD: below detection limit. [a]We used $\delta^{11}B$ (−2.0‰) and B/Al (3,775.5 µmole/mole) values from S6 in 23C-M to calculate the B contribution from silicate phases. [b]Results from ExA were used. [c]Results from ExB were used.

50%-carb-2 sample, which has 11 mg carbonate, by scaling down the reagent volume to 0.75 ml per step (i.e., a reagent to carbonate ratio of ~0.07 ml/mg, Figure 6a). This same reagent to carbonate ratio was also successfully applied to the larger 21 mg carbonate 50%-carb-3 sample, using 1.5 ml reagent per step, and to the smaller 5 mg carbonate 25%-carb sample, using 0.375 ml reagent per step (see Table 3 and Figure 6a). Alternatively, it is possible that reagent concentration might be scaled with carbonate mass, which might be useful in some cases to ensure sufficient solution volumes are maintained to allow efficient mixing with the solid sample, but this has not been tested here.

### 4.3. Elemental Composition and $\delta^{11}B$ Values for the MDAC Samples From the Norwegian Margin

Through the investigation of the B sources from the different leaching steps, we can calculate representative elemental ratios and B isotopic values for the carbonate portions of the 11 MDAC samples investigated (excluding silicate-dominated 23C-M; Table 4). The data that were chosen for this calculation typically represent steps containing less than 1 μg of Al in a volume of 0.8–1.6 ml leachate (Table 4). The $\delta^{11}B$ values range from 6.9 to 13.5‰ with the highest value from CFC-A10 (Barents Sea) and the lowest from MC-4CC-M (Vestnesa Ridge) (Table 4). The B/Ca ratios range from 20 to 72 μmol/mol with the highest ratio also observed in CFC-A10 (Barents Sea) and the lowest from MC-12R-M (Vestnesa Ridge).

When comparing the B/Ca ratios and $\delta^{11}B$ values derived with the sequential leaching method to those obtained by single-step HNO_3 leaching (0.1 M HNO_3; Table 1), we observe significantly higher $\delta^{11}B$ and lower B/Ca ratios in the sequential leaching. Four of our samples (CFC-A10, MC-M13, MC-M4, and MC-M5) have been treated with a single-step HNO_3 leaching, with buffer and oxidative cleaning steps identical to the sequential leaching. The resulting $\delta^{11}B$ and B/Ca ratios range from 2.5 to 11.6‰ and 64 to 98 μmole/mole, respectively (Data Set S2, https://doi.org/10.60520/IEDA/113483). The low recovery of boron (4.1%–8.3%, Table 1) and high Al/Ca ratios (14–5,994 μmole/mole) in the leachate after such a single-step treatment evidently suggest high contributions of boron from silicate phases as compared to the results of sequential leaching. We therefore recommend against such single-step treatment for obtaining genuine boron signatures of marine carbonate from impure samples.

The small amounts of Al detected in steps S1–S6 of the sequential leaching protocol suggest trace contributions from silicate minerals affect all leaching steps (Table 4). We calculated the "silicate-free" $\delta^{11}B$, B/Ca, and Mg/Ca values in MDAC by assuming a binary mixing between the carbonate and silicate phases. We assumed that all the Al detected is from a silicate-rich end member, whose composition can be represented by the results from sample 23C-M (with values listed in Table 4). This assumption can be justified by the observations that $\delta^{11}B$ and Mg/Ca values from concentrated acid leaching seem to trend toward similar values to that from 23C-M (Figures 11c and 11e). We then are able to calculate the silicate contribution to the chosen leachate steps, which ranges from less than 0.01% in 12R-A to 12.1% in 8B (Table 4). The largest changes in $\delta^{11}B$ and B/Ca ratios are observed in 8B, with an increase of 1.8‰ and a decrease of 2.9 μmole/mole, respectively.

We compared the $\delta^{11}B$ values and elemental ratios from all the leaching steps (Figure 11), as well as the "silicate-free" values, by grouping samples according to their mineral composition as defined by the XRD (Figure 3). The composition from sample CFC-12R-A likely represents the aragonitic end member, as this sample contains almost exclusively aragonite (87%; Figure 3 and Table 2). The Mg-calcite end member can be represented by sample MC-18A, which contains the most Mg-calcite (44%) (Figure 3 and Table 2). Sample 23C-M represents the non-carbonate end member, with mostly quartz and a few percent of K-feldspar, mica, and chlorite (Figure 3 and Table 2). Results from all leaching steps from these three end member compositions were plotted on the $\delta^{11}B$ versus Mg/Ca and B/Ca versus Mg/Ca cross plots (Figure 11).

Two patterns emerge when comparing the mineral composition with elemental ratios. First, the variation in carbonate mineralogy is reflected by the Mg/Ca ratios for the Group 1 samples (i.e., >50% silicates with variable proportions of aragonite and Mg-calcite). As shown in Figure 11c, the highest Mg/Ca ratio ($\sim 10^2$ mmol/mol) is observed in sample MC-18A (i.e., the Mg-calcite end-member) while the lowest ratio ($\sim 10^0$ mmole/mole) is observed in the aragonite end-member sample CFC-12R-A. Moderate ratios ($\sim 10^1$ mmole/mole) are observed in three samples that consist of variable amounts of Mg-calcite and aragonite (MC-8B, MC-M5, and MC-M4; Figures 11c and 11d). Such a pattern provides confidence that the variation in mineral composition is well reflected by the elemental data obtained from our sequential leaching treatment.
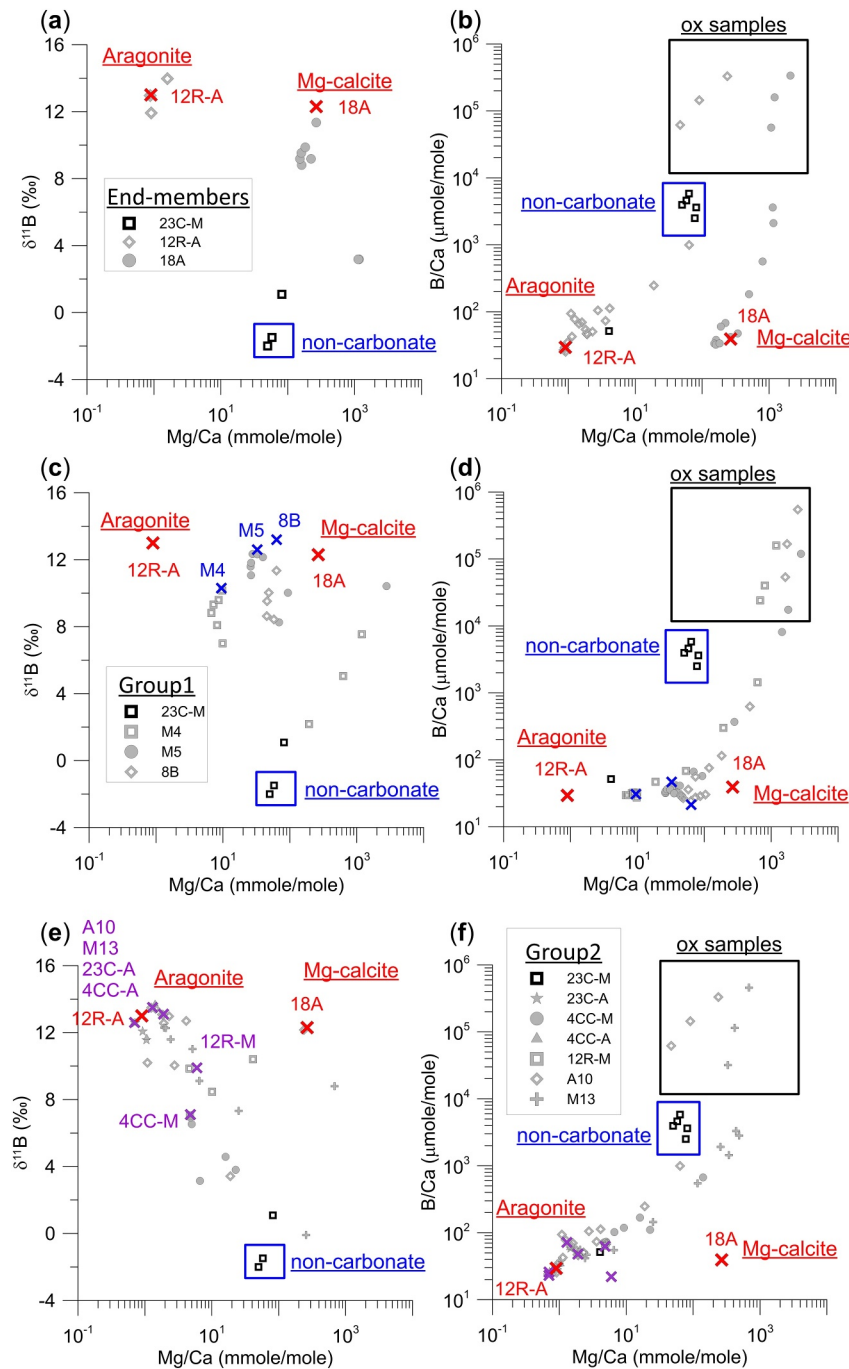
Figure 11. Cross plots of $\delta^{11}B$ versus Mg/Ca and B/Ca versus Mg/Ca for all steps, including the oxidative cleaning and buffer cleaning. Red, blue, and purple crosses indicate the corrected values for silicate contamination (Table 4) whereas gray and black symbols indicate the uncorrected values for the different samples. (a and b) Composition of the aragonite, Mg-calcite, and non-carbonate end-members as represented by the MDAC samples CFC-12R-A and MC-18A as well as the background sample 23C-M, respectively. The aragonite and Mg-calcite end-members can be clearly separated by their Mg/Ca ratios, which provide confidence to our leaching results. The non-carbonate end-member is characterized by the very low $\delta^{11}B$ values. The *ox* samples are characterized by very high B/Ca ratios with $\delta^{11}B$ range from 7.6 to 12.2‰ (*n* = 4). (c and d) Leachate composition for the Group 1 MDAC samples (MC-M4, MC-M5 MC-8B) that have more than 50% detrital minerals and variable fractions of aragonite and Mg-calcite (Figure 3). Their Mg/Ca ratios clearly reflect such a mixture of carbonate minerals with variable influences from the non-carbonate end-member in the different steps of acid leaching as indicated by the $\delta^{11}B$ signatures and B/Ca ratios. (e and f) Leachate composition from the Group 2 samples (CFC-23C-A, MC-4CC-M, CFC-4CC-A, CFC-12R-A, CFC-A10, and MC-M13) that are composed almost exclusively of aragonite (Table 4). Four of the samples in Group 2 have values very similar to the aragonite end-member. The samples MC-12R-M and MC-4CC-M show much lower $\delta^{11}B$ values compared to the aragonitic end-member.

The second pattern that emerges is a trend of decreasing $\delta^{11}B$ values and increasing Mg/Ca ratios among the different leaching steps of a given sample toward the values representing the non-carbonate end-member (Figures 11c and 11e). Leachates from oxidative cleaning and concentrated-acid leaching (especially for S9 and S10) have moderate Mg/Ca ($\sim 10^1$ mmole/mole) and low $\delta^{11}B$ (<0‰). A similar pattern can also be observed from the B/Ca versus Mg/Ca cross plot (Figures 11d and 11e) with trends toward high B/Ca ratios for samples from oxidative cleaning and concentrated HAc leaching. This observation supports our earlier inferences that silicate mineral decomposition occurs not only during the concentrated HAc leaching but also during the oxidative cleaning.

The trend toward the non-carbonate end member is particularly pronounced in a few samples from Group 2 (e.g., MC-12R-M and MC-4CC-M; Figure 11e). Such a mixing trend is perhaps surprising as fewer non-carbonate minerals were detected in this group by XRD as compared to Group 1 (Figure 3). A likely explanation is that the degree of mixing in $\delta^{11}B$ toward the non-carbonate end member also depends on the type of silicate minerals. For example, samples MC-4CC-M and MC-12R-M happen to have the most abundant mica (5.9% and 6.7%; Table 2) as compared to all the other samples (0.4%–2.9%; Table 2). Phyllosilicates are known to contain more boron than other silicate minerals. For example, in metapelitic and granitic rocks, muscovite contains one to two orders of magnitude more boron compared to chlorite, plagioclase, and feldspar (Gaillardet & Lemarchand, 2018). The dissolution of these phyllosilicates (such as mica) maybe promoted during the formation of MDAC as proposed by Hong et al. (2022) as a result of increasing acidity during anaerobic oxidation of methane can carbonate formation in the micro-environment. The released boron during phyllosilicate dissolution with low $\delta^{11}B$ values was later incorporated into MDAC and results in the trends observed from samples in Group 2.

5. Conclusions

We developed and calibrated a sequential leaching method to separate the different boron-hosting phases from geological archives such as the notoriously heterogeneous MDAC samples. Based on the $\delta^{11}B$ values and elemental ratios, we are able to determine the most likely sources of boron in each leaching treatment (oxidative cleaning, buffer cleaning, and HAc leaching). The low $\delta^{11}B$ values and high Al concentrations obtained during the oxidative cleaning steps suggest significant contributions from silicate mineral decomposition, alongside the boron released from organic matter decomposition. For the buffer cleaning steps, most of the boron in the leachate is from clay desorption, with co-occurring carbonate decomposition during such treatment suggested by appreciable Ca concentrations measured in the leachate. During the first few leaching steps with diluted HAc (0.25 vol%), despite the increasing dissolution of carbonate, $\delta^{11}B$ values may still reflect the influence of boron sourced from non-carbonate phases. The most representative boron signal from carbonate is derived when ca. 30%–40% of the carbonate is dissolved, which is indicated by the highest $\delta^{11}B$ values and a maximum in Ca concentration. In the MDAC samples this is found in the steps with moderate HAc strength (i.e., S3–S6), while in the artificial clay-carbonate mixtures, representative $\delta^{11}B$ values are already observed in the first two HAc leaching steps. In the last few steps with strong HAc leaching (S7–S10), silicate dissolution dominates the release of boron into the leachate. This is evident from the exponential increase of Al/Ca ratios in the leachate and anomalously low $\delta^{11}B$ values.

After treating 11 MDAC samples from three cold seeps along the Norwegian margin with the sequential leaching procedure, we are able to obtain $\delta^{11}B$ values and elemental ratios that reflect the carbonate composition represented by the step(s) with highest $\delta^{11}B$ values. The Mg/Ca ratios derived reflect the different mixtures of carbonates (e.g., Mg-calcite and aragonite) in the MDAC samples and agree well with the XRD investigations. We further demonstrate how the amount of sample material and volume of acid used (or different sample-to-acid ratios) affect the performance of the sequential leaching. Knowing the amounts of carbonate in the samples before leaching treatment is thus important for optimizing leaching efficiency. We obtained optimal results with reagent-to-carbonate ratios between 0.069 and 0.100 ml/mg $CaCO_3$. For samples with lower quantity of carbonate, the reagent volume (or potentially strength) should be scaled down for optimization of carbonate leaching. In conclusion, sequential leaching of B from impure carbonate rocks is a viable technique for extracting carbonate-bound $\delta^{11}B$ data.

Data Availability Statement

Data produced in this paper can be accessed at the Interdisciplinary Earth Data Alliance (Hong et al., 2024).

References

Bailey, T. R., McArthur, J. M., Prince, H., & Thirlwall, M. F. (2000). Dissolution methods for strontium isotope stratigraphy: Whole rock analysis. *Chemical Geology*, *167*(3–4), 313–319. https://doi.org/10.1016/S0009-2541(99)00235-1

Bellefroid, E. J., Planavsky, N. J., Miller, N. R., Brand, U., & Wang, C. (2018). Case studies on the utility of sequential carbonate leaching for radiogenic strontium isotope analysis. *Chemical Geology*, *497*, 88–99. https://doi.org/10.1016/j.chemgeo.2018.08.025

Crémière, A., Lepland, A., Chand, S., Sahy, D., Condon, D. J., Noble, S. R., et al. (2016). Timescales of methane seepage on the Norwegian margin following collapse of the Scandinavian Ice Sheet. *Nature Communications*, *7*(1), 1–10. https://doi.org/10.1038/ncomms11509

Dellinger, M., Hardisty, D. S., Planavsky, N. J., Gill, B. C., Kalderon-Asael, B., Asael, D., et al. (2020). The effects of diagenesis on lithium isotope ratios of shallow marine carbonates. *American Journal of Science*, *320*(2), 150–184. https://doi.org/10.2475/02.2020.03

Deyhle, A., & Kopf, A. (2001). Deep fluids and ancient pore waters at the backstop: Stable isotope systematics (B, C, O) of mud-volcano deposits on the Mediterranean Ridge accretionary wedge. *Geology*, *29*(11), 1031. https://doi.org/10.1130/0091-7613(2001)029<1031:DFAAPW>2.0.CO;2

Deyhle, A., & Kopf, A. (2004). Possible influence of clay contamination on B isotope geochemistry of carbonaceous samples. *Applied Geochemistry*, *19*(5), 737–745. https://doi.org/10.1016/j.apgeochem.2003.10.008

Foster, G. L. (2008). Seawater pH, pCO$_2$ and [CO$_3^{2-}$] variations in the Caribbean Sea over the last 130 kyr: A boron isotope and B/Ca study of planktic foraminifera. *Earth and Planetary Science Letters*, *271*(1–4), 254–266. https://doi.org/10.1016/j.epsl.2008.04.015

Foster, G. L., Hönisch, B., Paris, G., Dwyer, G. S., Rae, J. W. B., Elliott, T., et al. (2013). Interlaboratory comparison of boron isotope analyses of boric acid, seawater and marine CaCO$_3$ by MC-ICPMS and NTIMS. *Chemical Geology*, *358*, 1–14. https://doi.org/10.1016/j.chemgeo.2013.08.027

Foster, G. L., & Rae, J. W. B. (2016). Reconstructing ocean pH with boron isotopes in foraminifera. *Annual Review of Earth and Planetary Sciences*, *44*(1), 207–237. https://doi.org/10.1146/annurev-earth-060115-012226

Gagnon, A. C., Gothmann, A. M., Branson, O., Rae, J. W. B., & Stewart, J. A. (2021). Controls on boron isotopes in a cold-water coral and the cost of resilience to ocean acidification. *Earth and Planetary Science Letters*, *554*, 116662. https://doi.org/10.1016/j.epsl.2020.116662

Gaillardet, J., & Lemarchand, D. (2018). Boron in the weathering environment. *Advances in Isotope Geochemistry*, 163–188. https://doi.org/10.1007/978-3-319-64666-4_7/COVER

Gutjahr, M., Bordier, L., Douville, E., Farmer, J., Foster, G. L., Hathorne, E. C., et al. (2021). Sub-permil interlaboratory consistency for solution-based boron isotope analyses on marine carbonates. *Geostandards and Geoanalytical Research*, *45*(1), 59–75. https://doi.org/10.1111/ggr.12364

Hemming, N. G., & Hanson, G. N. (1992). Boron isotopic composition and concentration in modern marine carbonates. *Geochimica et Cosmochimica Acta*, *56*(1), 537–543. https://doi.org/10.1016/0016-7037(92)90151-8

Himmler, T., Bach, W., Bohrmann, G., & Peckmann, J. (2010). Rare Earth elements in authigenic methane-seep carbonates as tracers for fluid composition during early diagenesis. *Chemical Geology*, *277*(1–2), 126–136. https://doi.org/10.1016/j.chemgeo.2010.07.015

Hong, W.-L., Lepland, A., Crémière, A., Kirsimäe, K., Stüeken, E. E., Dumont, M., et al. (2024). Changes in mineral and leachate (major, minor, and boron isotope) composition during sequential extraction of authigenic carbonate. Version 1.0 [Dataset]. *Interdisciplinary Earth Data Alliance (IEDA)*. https://doi.org/10.60520/IEDA/113483

Hong, W.-L., Lepland, A., Kirsimäe, K., Crémière, A., & Rae, J. W. B. (2022). Boron concentrations and isotopic compositions in methane-derived authigenic carbonates: Constraints and limitations in reconstructing formation conditions. *Earth and Planetary Science Letters*, *579*, 117337. https://doi.org/10.1016/J.EPSL.2021.117337

Hönisch, B., Eggins, S. M., Haynes, L. L., Allen, K. A., Holland, K. D., & Lorbacher, K. (2019). Boron proxies in paleoceanography and paleoclimatology. In *Boron proxies in paleoceanography and paleoclimatology*. John Wiley & Sons, Ltd. https://doi.org/10.1002/9781119010678

Hosking, J. S. (1932). The influence of hydrogen-ion concentration on the decomposition of soil organic matter by hydrogen peroxide. *The Journal of Agricultural Science*, *22*(1), 92–100. https://doi.org/10.1017/S0021859600053119

Ishikawa, T., & Nakamura, E. (1993). Boron isotope systematics of marine sediments. *Earth and Planetary Science Letters*, *117*(3–4), 567–580.

Joseph, C., Campbell, K. A., Torres, M. E., Martin, R. A., Pohlman, J. W., Riedel, M., & Rose, K. (2013). Methane-derived authigenic carbonates from modern and paleoseeps on the Cascadia margin: Mechanisms of formation and diagenetic signals. *Palaeogeography, Palaeoclimatology, Palaeoecology*, *390*, 52–67. https://doi.org/10.1016/j.palaeo.2013.01.012

Jurikova, H., Liebetrau, V., Gutjahr, M., Rollion-Bard, C., Hu, M. Y., Krause, S., et al. (2019). Boron isotope systematics of cultured brachiopods: Response to acidification, vital effects and implications for palaeo-pH reconstruction. *Geochimica et Cosmochimica Acta*, *248*, 370–386. https://doi.org/10.1016/j.gca.2019.01.015

Kasemann, S. A., Prave, A. R., Fallick, A. E., Hawkesworth, C. J., & Hoffmann, K. H. (2010). Neoproterozoic ice ages, boron isotopes, and ocean acidification: Implications for a snowball Earth. *Geology*, *38*(9), 775–778. https://doi.org/10.1130/G30851.1

Kiss, E. (1988). Ion-exchange separation and spectrophotometric determination of boron in geological materials. *Analytica Chimica Acta*, *211*(C), 243–256. https://doi.org/10.1016/S0003-2670(00)83684-3

Lemarchand, E., Schott, J., & Gaillardet, J. (2005). Boron isotopic fractionation related to boron sorption on humic acid and the structure of surface complexes formed. *Geochimica et Cosmochimica Acta*, *69*(14), 3519–3533. https://doi.org/10.1016/j.gca.2005.02.024

Li, D., Shields-Zhou, G. A., Ling, H.-F., & Thirlwall, M. (2011). Dissolution methods for strontium isotope stratigraphy: Guidelines for the use of bulk carbonate and phosphorite rocks. *Chemical Geology*, *290*(3), 133–144. https://doi.org/10.1016/j.chemgeo.2011.09.004

Liu, C., Wang, Z., & Raub, T. D. (2013). Geochemical constraints on the origin of Marinoan cap dolostones from Nuccaleena Formation, South Australia. *Chemical Geology*, *351*, 95–104. https://doi.org/10.1016/j.chemgeo.2013.05.012

Magalhães, V. H., Pinheiro, L. M., Ivanov, M. K., Kozlova, E., Blinova, V., Kolganova, J., et al. (2012). Formation processes of methane-derived authigenic carbonates from the Gulf of Cadiz. *Sedimentary Geology*, *243–244*, 155–168. https://doi.org/10.1016/j.sedgeo.2011.10.013

McCulloch, M. T., D'Olivo, J. P., Falter, J., Georgiou, L., Holcomb, M., Montagna, P., & Trotter, J. A. (2018). Boron isotopic systematics in scleractinian corals and the role of pH up-regulation. In *Advances in isotope geochemistry* (pp. 145–162). Springer. https://doi.org/10.1007/978-3-319-64666-4_6

Mikutta, R., Kleber, M., & Jahn, R. (2005). Poorly crystalline minerals protect organic carbon in clay subfractions from acid subsoil horizons. In *Geoderma* (Vol. 128, pp. 106–115). Elsevier. https://doi.org/10.1016/j.geoderma.2004.12.018

Mikutta, R., Kleber, M., Kaiser, K., & Jahn, R. (2005). Review: Organic matter removal from soils using hydrogen peroxide, sodium hypochlorite, and disodium peroxodisulfate. *Soil Science Society of America Journal*, 69(1), 120–135. https://doi.org/10.2136/sssaj2005.0120

Misra, S., Greaves, M., Owen, R., Kerr, J., Elmore, A. C., & Elderfield, H. (2014). Determination of B/Ca of natural carbonates by HR-ICP-MS. *Geochemistry, Geophysics, Geosystems*, 15(4), 1617–1628. https://doi.org/10.1002/2013GC005049

Ni, Y., Foster, G. L., Bailey, T., Elliott, T., Schmidt, D. N., Pearson, P., et al. (2007). A core top assessment of proxies for the ocean carbonate system in surface-dwelling foraminifers. *Paleoceanography*, 22(3). https://doi.org/10.1029/2006PA001337

Palmer, M. R., Spivack, A. J., & Edmond, J. M. (1987). Temperature and pH controls over isotopic fractionation during adsorption of boron on marine clay. *Geochimica et Cosmochimica Acta*, 51(9), 2319–2323. https://doi.org/10.1016/0016-7037(87)90285-7

Paris, G., Bartolini, A., Donnadieu, Y., Beaumont, V., & Gaillardet, J. (2010). Investigating boron isotopes in a middle Jurassic micritic sequence: Primary vs. diagenetic signal. *Chemical Geology*, 275(3–4), 117–126. https://doi.org/10.1016/j.chemgeo.2010.03.013

Peckmann, J., Thiel, V., Michaelis, W., Clari, P., Gaillard, C., Martire, L., & Reitner, J. (1999). Cold seep deposits of Beauvoisin (Oxfordian; southeastern France) and Marmorito (Miocene; northern Italy): Microbially induced authigenic carbonates. *International Journal of Earth Sciences*, 88(1), 60–75. https://doi.org/10.1007/S005310050246

Phillips, S. C., Hong, W. L., Johnson, J. E., Fahnestock, M. F., & Bryce, J. G. (2018). Authigenic carbonate formation influenced by freshwater inputs and methanogenesis in coal-bearing strata offshore Shimokita, Japan (IODP site C0020). *Marine and Petroleum Geology*, 96, 288–303. https://doi.org/10.1016/j.marpetgeo.2018.06.007

Phillips, S. C., Johnson, J. E., Giosan, L., & Rose, K. (2014). Monsoon-influenced variation in productivity and lithogenic sediment flux since 110ka in the offshore Mahanadi Basin, northern Bay of Bengal. *Marine and Petroleum Geology*, 58, 502–525. https://doi.org/10.1016/j.marpetgeo.2014.05.007

Rae, J. W. B. (2018). Boron isotopes in foraminifera: Systematics, biomineralisation, and CO_2 reconstruction. In *Advances in isotope geochemistry* (pp. 107–143). Springer. https://doi.org/10.1007/978-3-319-64666-4_5

Rae, J. W. B., Foster, G. L., Schmidt, D. N., & Elliott, T. (2011). Boron isotopes and B/Ca in benthic foraminifera: Proxies for the deep ocean carbonate system. *Earth and Planetary Science Letters*, 302(3–4), 403–413. https://doi.org/10.1016/j.epsl.2010.12.034

Shao, J., Stott, L. D., Gray, W. R., Greenop, R., Pecher, I., Neil, H. L., et al. (2019). Atmosphere-ocean CO_2 exchange across the last deglaciation from the boron isotope proxy. *Paleoceanography and Paleoclimatology*, 34(10), 1650–1670. https://doi.org/10.1029/2018PA003498

Steiner, Z., Rae, J. W. B., Berelson, W. M., Adkins, J. F., Hou, Y., Dong, S., et al. (2022). Authigenic formation of clay minerals in the Abyssal North Pacific. *Global Biogeochemical Cycles*, 36(11), e2021GB007270. https://doi.org/10.1029/2021GB007270

Stewart, J. A., Christopher, S. J., Kucklick, J. R., Bordier, L., Chalk, T. B., Dapoigny, A., et al. (2021). NIST RM 8301 boron isotopes in marine carbonate (simulated coral and foraminifera solutions): Inter-laboratory $\delta^{11}B$ and trace element ratio value assignment. *Geostandards and Geoanalytical Research*, 45(1), 77–96. https://doi.org/10.1111/ggr.12363

Stewart, J. A., Gutjahr, M., Pearce, F., Swart, P. K., & Foster, G. L. (2015). Boron during meteoric diagenesis and its potential implications for Marinoan snowball Earth $\delta^{11}B$-pH excursions. *Geology*, 43(7), 627–630. https://doi.org/10.1130/G36652.1

Taylor, H. L., Kell Duivestein, I. J., Farkas, J., Dietzel, M., & Dosseto, A. (2019). Technical note: Lithium isotopes in dolostone as a palaeo-environmental proxy-An experimental approach. *Climate of the Past*, 15(2), 635–646. https://doi.org/10.5194/CP-15-635-2019

Teichert, B. M. A., Eisenhauer, A., Bohrmann, G., Haase-Schramm, A., Bock, B., & Linke, P. (2003). U/Th systematics and ages of authigenic carbonates from Hydrate Ridge, Cascadia Margin: Recorders of fluid flow variations. *Geochimica et Cosmochimica Acta*, 67(20), 3845–3857. https://doi.org/10.1016/S0016-7037(03)00128-5

Trudgill, M., Nuber, S., Block, H. E., Crumpton-Banks, J., Jurikova, H., Littley, E., et al. (2024). A simple, low-blank batch purification method for high-precision boron isotope analysis. *Geochemistry, Geophysics, Geosystems*, 25(3), e2023GC011350. https://doi.org/10.1029/2023gc011350

Vogl, J., & Rosner, M. (2012). Production and certification of a unique set of isotope and delta reference materials for boron isotope determination in geochemical, environmental and industrial materials. *Geostandards and Geoanalytical Research*, 36(2), 161–175. https://doi.org/10.1111/j.1751-908X.2011.00136.x

Voinot, A., Lemarchand, D., Collignon, C., Granet, M., Chabaux, F., & Turpault, M. P. (2013). Experimental dissolution vs. transformation of micas under acidic soil conditions: Clues from boron isotopes. *Geochimica et Cosmochimica Acta*, 117, 144–160. https://doi.org/10.1016/j.gca.2013.04.012

Xu, C., Jurikova, H., Nuber, S., Steele, R. C. J., Trudgill, M., Barker, S., et al. (2024). A rapid, simple, and low-blank pumped ion-exchange column chromatography technique for boron purification from carbonate and seawater matrices. *Geochemistry, Geophysics, Geosystems*, 25(2), e2023GC011228. https://doi.org/10.1029/2023GC011228

Yoshimura, K., Miyazaki, Y., Ota, F., Matsuoka, S., & Sakashita, H. (1998). Complexation of boric acid with the N-methyl-D-glucamine group in solution and in crosslinked polymer. *Journal of the Chemical Society - Faraday Transactions*, 94(5), 683–689. https://doi.org/10.1039/a707790d

Zeebe, R. E., & Rae, J. W. B. (2020). Equilibria, kinetics, and boron isotope partitioning in the aqueous boric acid–hydrofluoric acid system. *Chemical Geology*, 550, 119693. https://doi.org/10.1016/j.chemgeo.2020.119693

Zhang, S., Henehan, M. J., Hull, P. M., Reid, R. P., Hardisty, D. S., Hood, A. V. S., & Planavsky, N. J. (2017). Investigating controls on boron isotope ratios in shallow marine carbonates. *Earth and Planetary Science Letters*, 458, 380–393. https://doi.org/10.1016/j.epsl.2016.10.059